ACADEMIC PRESS

Available online at www.sciencedirect.com

SCIENCE DIRECT®

Journal of Sound and Vibration 264 (2003) 1091–1125

JOURNAL OF SOUND AND VIBRATION

www.elsevier.com/locate/jsvi

A comparison of shell theories for large-amplitude vibrations of circular cylindrical shells: Lagrangian approach

M. Amabili*

Dipartimento di Ingegneria Industriale, Università di Parma, Parco Area delle Scienze 181/A, Parma 43100, Italy

Received 11 March 2002; accepted 6 June 2002

Abstract

Large-amplitude (geometrically non-linear) vibrations of circular cylindrical shells subjected to radial harmonic excitation in the spectral neighbourhood of the lowest resonances are investigated. The Lagrange equations of motion are obtained by an energy approach, retaining damping through Rayleigh's dissipation function. Four different non-linear thin shell theories, namely Donnell's, Sanders–Koiter, Flügge–Lur'e-Byrne and Novozhilov's theories, which neglect rotary inertia and shear deformation, are used to calculate the elastic strain energy. The formulation is also valid for orthotropic and symmetric cross-ply laminated composite shells. The large-amplitude response of perfect and imperfect, simply supported circular cylindrical shells to harmonic excitation in the spectral neighbourhood of the lowest natural frequency is computed for all these shell theories. Numerical responses obtained by using these four non-linear shell theories are also compared to results obtained by using the Donnell's non-linear shallow-shell equation of motion. A validation of calculations by comparison with experimental results is also performed. Both empty and fluid-filled shells are investigated by using a potential fluid model. The effects of radial pressure and axial load are also studied. Boundary conditions for simply supported shells are exactly satisfied. Different expansions involving from 14 to 48 generalized co-ordinates, associated with natural modes of simply supported shells, are used. The non-linear equations of motion are studied by using a code based on an arclength continuation method allowing bifurcation analysis.

1. Introduction

A large number of studies on large-amplitude (geometrically non-linear) vibrations of circular cylindrical shells is available (see the extensive review of Amabili and Païdoussis [1]). A good percentage of them address large-amplitude free and forced vibrations under radial harmonic

*Tel.: 39-0521-905-896; fax: +39-0521-905-705.
E-mail address: marco@me.unipr.it (M. Amabili).

0022-460X/03/$ - see front matter
doi:10.1016/S0022-460X(02)01385-8

excitation. Most of these studies used the Donnell's non-linear shallow-shell theory to obtain the equations of motion; see, e.g. Ref. [2–11]. Only a few used the more refined Sanders–Koiter (also referred to as Sanders) non-linear shell theory [12–20] and only one the Flügge–Lur'e-Byrne (also referred to as modified Flügge) non-linear shell theory [21]. The majority of these studies do not include geometric imperfections and some of them use a single-mode approximation to describe the shell dynamics. The Novozhilov's non-linear shell theory was used only by Mente [22] to investigate the response of circular cylindrical shells under asymmetric transient load (air blast). Sansour et al. [23,24] developed a finite element approach with a refined shell theory and integration algorithm, only applied to study the response of a circular cylindrical panel to a harmonic excitation with a single, fixed frequency. Refined shell theories developed for thick and composite laminated shells, as the first order shear deformation theory [25] and the non-linear parabolic shear deformation theory [26], have been applied only to study static and transient responses, except Kobayashi and Leissa [27] who studied free vibrations of doubly curved panels.

Some of the studies based on Donnell's non-linear shallow-shell theory present very refined mode expansions and analysis of the shell response, but the accuracy of results can be questioned because this shell theory is usually indicated as not particularly accurate. Similar results with more refined shell theories are not yet available. Moreover, a comparison of the non-linear shell response in the frequency range around a resonance computed by using different shell theories would be fundamental to quantify and discuss possible differences.

The only comparison available in the literature for shell responses computed by using different shell theories, specifically (i) Donnell's non-linear theory (without the shallow-shell hypothesis, i.e., retaining in-plane inertia), (ii) Novozhilov non-linear shell theory and (iii) a simplified version of the Sanders–Koiter non-linear theory, was performed by Mente [22]. However, this comparison was done for a transient response of a shell, and it is not possible to make any deduction on the different trends of non-linearity obtained by using different shell theories. Taking Novozhilov's theory as reference, results obtained by using Sanders–Koiter theory compared very closely (within 1%), while those obtained by Donnell's theory predicted a 4% or 5% larger response with less time to reach the maximum response. Moreover, the study by Mente was performed when knowledge of shell non-linear dynamics and computational tools were limited with respect to present days.

The present study has the aim of filling this gap existing in the literature by presenting a comparison of shell response to radial harmonic excitation in the spectral neighbourhood of the lowest natural frequency computed by using five different non-linear shell theories: (i) Donnell's shallow-shell, (ii) Donnell's with in-plane inertia, (iii) Sanders–Koiter, (iv) Flügge–Lur'e-Byrne and (v) Novozhilov's theories. Actually, for the last two shell theories, more refined formulations have been obtained in the present study, retaining non-linear effects in the change of curvature and torsion in the Flügge–Lur'e-Byrne theory and delaying the thinness assumption for the Novozhilov's theory. These five shell theories are practically the only ones generally applied to geometrically non-linear problems among the theories that use only three variables, which are the three middle surface displacements. More complicated shell theories (e.g. see Ref. [25]), suitable for moderately thick laminated shells exist, but are not considered in the present study because they use five independent variables, three displacements and two rotations.

The Lagrange equations of motion are obtained by an energy approach, retaining damping through Rayleigh's dissipation function. The formulation is also valid for orthotropic and symmetric cross-ply laminated composite shells. A validation of calculations by comparison with

experimental results is also performed. Both empty and fluid-filled shells are investigated by using a potential fluid model. The effects of radial pressure and axial loads on the non-linear response are also studied. Boundary conditions for simply supported shells are exactly satisfied. Different expansions involving from 14 to 48 generalized co-ordinates, associated to natural modes of simply supported shells, are used. The non-linear equations of motion are studied by using a code based on arclength continuation method that allows bifurcation analysis.

2. Elastic strain energy of the shell according to (i) Donnell (ii) Sanders–Koiter, (iii) Flügge–Lur'e-Byrne and (iv) Novozhilov Theories

Fig. 1 shows a circular cylindrical shell with the cylindrical co-ordinate system (O; x, r, θ), having the origin O at the centre of one end of the shell. The displacements of an arbitrary point of coordinates (x, θ) on the middle surface of the shell are denoted by u, v and w, in the axial, circumferential and radial directions, respectively; w is taken positive outwards. Initial imperfections of the circular cylindrical shell associated with zero initial tension are denoted by radial displacement w_0, also positive outwards; only radial initial imperfections are considered.

Four different strain–displacement relationships for thin shells are used in the present study, in order to compare results. They are based on Love's first approximation assumptions: (i) the shell thickness h is small with respect to the radius of curvature R of the middle plane; (ii) strains are small; (iii) transverse normal stress is small; and (iv) the Kirchhoff–Love kinematic hypothesis, in which it is assumed that the normal to the undeformed middle surface remains straight and normal to the midsurface after deformation, and undergoes no thickness stretching. These shell theories are: (i) Donnell's [28], (ii) Sanders–Koiter [13,28,29], (iii) Flügge–Lur'e-Byrne [21,28] (also referred to as modified Flügge in Ref. [28]) and (iv) Novozhilov's [30] non-linear shell theories. For all of them, rotary inertia and shear deformations are neglected. According to these shell theories, the strain components ε_x, ε_θ and $\gamma_{x\theta}$ at an arbitrary point of the shell are related to

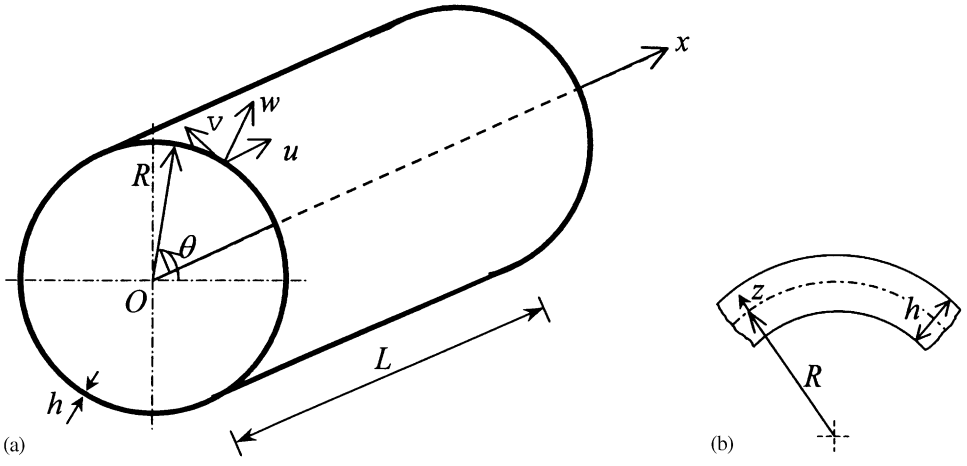

Fig. 1. Co-ordinate system and dimensions for circular cylindrical shell (a) complete shell; (b) cross-section of the shell surface.

the middle surface strains $\varepsilon_{x,0}$, $\varepsilon_{\theta,0}$ and $\gamma_{x\theta,0}$ and to the changes in the curvature and torsion of the middle surface k_x, k_θ and $k_{x\theta}$ by the following three relationships [28]:

$$\varepsilon_x = \varepsilon_{x,0} + zk_x, \quad \varepsilon_\theta = \varepsilon_{\theta,0} + zk_\theta, \quad \gamma_{x\theta} = \gamma_{x\theta,\,0} + zk_{x\theta} \tag{1a–c}$$

where z is the distance of the arbitrary point of the shell from the middle surface (see Fig. 1(b)).

According to Donnell's non-linear shell theory, the middle surface strain-displacement relationships and changes in the curvature and torsion are obtained for a circular cylindrical shell [28]

$$\varepsilon_{x,0} = \frac{\partial u}{\partial x} + \frac{1}{2}\left(\frac{\partial w}{\partial x}\right)^2 + \frac{\partial w}{\partial x}\frac{\partial w_0}{\partial x}, \tag{2a}$$

$$\varepsilon_{\theta,0} = \frac{\partial v}{R\partial\theta} + \frac{w}{R} + \frac{1}{2}\left(\frac{\partial w}{R\partial\theta}\right)^2 + \frac{\partial w}{R\partial\theta}\frac{\partial w_0}{R\partial\theta}, \tag{2b}$$

$$\gamma_{x\theta,0} = \frac{\partial u}{R\partial\theta} + \frac{\partial v}{\partial x} + \frac{\partial w}{\partial x}\frac{\partial w}{R\partial\theta} + \frac{\partial w}{\partial x}\frac{\partial w_0}{R\partial\theta} + \frac{\partial w_0}{\partial x}\frac{\partial w}{R\partial\theta}, \tag{2c}$$

$$k_x = -\frac{\partial^2 w}{\partial x^2}, \tag{2d}$$

$$k_\theta = -\frac{\partial^2 w}{R^2\partial\theta^2}, \tag{2e}$$

$$k_{x\theta} = -2\frac{\partial^2 w}{R\partial x\partial\theta}. \tag{2f}$$

Sanders [31] developed a more refined non-linear theory of shells expressed in tensorial form; the same equations were obtained by Koiter [32] around the same period, leading to the designation of these equations as the Sanders–Koiter equations. The middle surface strain–displacement relationships, changes in the curvature and torsion in this case are [28,29]

$$\varepsilon_{x,0} = \frac{\partial u}{\partial x} + \frac{1}{2}\left(\frac{\partial w}{\partial x}\right)^2 + \frac{1}{8}\left(\frac{\partial v}{\partial x} - \frac{\partial u}{R\partial\theta}\right)^2 + \frac{\partial w}{\partial x}\frac{\partial w_0}{\partial x}, \tag{3a}$$

$$\varepsilon_{\theta,0} = \frac{\partial v}{R\partial\theta} + \frac{w}{R} + \frac{1}{2}\left(\frac{\partial w}{R\partial\theta} - \frac{v}{R}\right)^2 + \frac{1}{8}\left(\frac{\partial u}{R\partial\theta} - \frac{\partial v}{\partial x}\right)^2 + \frac{\partial w_0}{R\partial\theta}\left(\frac{\partial w}{R\partial\theta} - \frac{v}{R}\right), \tag{3b}$$

$$\gamma_{x\theta,0} = \frac{\partial u}{R\partial\theta} + \frac{\partial v}{\partial x} + \frac{\partial w}{\partial x}\left(\frac{\partial w}{R\partial\theta} - \frac{v}{R}\right) + \frac{\partial w_0}{\partial x}\left(\frac{\partial w}{R\partial\theta} - \frac{v}{R}\right) + \frac{\partial w}{\partial x}\frac{\partial w_0}{R\partial\theta}, \tag{3c}$$

$$k_x = -\frac{\partial^2 w}{\partial x^2}, \tag{3d}$$

$$k_\theta = \frac{\partial v}{R^2\partial\theta} - \frac{\partial^2 w}{R^2\partial\theta^2}, \tag{3e}$$

$$k_{x\theta} = -2\frac{\partial^2 w}{R\partial x\partial\theta} + \frac{1}{2R}\left(3\frac{\partial v}{\partial x} - \frac{\partial u}{R\partial\theta}\right). \tag{3f}$$

Changes in curvature and torsion are linear according to both Donnell's and Sanders–Koiter non-linear shell theories.

According to Flügge–Lur'e-Byrne non-linear theory [21,28], the thinness assumption is delayed in the derivations. For this reason, displacements $\tilde{u}$, $\tilde{v}$ and $\tilde{w}$ of points at distance z from the middle surface are introduced; they are related to displacements on the middle surface by the relationships [21,28]

$$\tilde{u} = u - z\frac{\partial(w+w_0)}{\partial x}, \quad \tilde{v} = v - \frac{z}{R}\left(\frac{\partial(w+w_0)}{\partial\theta} - v\right), \quad \tilde{w} = w + w_0. \tag{4a-c}$$

Eq. (4) are a simplified version of those obtained by Novozhilov [30]. The strain–displacement relationships for a generic point of the shell are [21,28]

$$\varepsilon_x = \frac{\partial\tilde{u}}{\partial x} + \frac{1}{2}\left[\left(\frac{\partial\tilde{u}}{\partial x}\right)^2 + \left(\frac{\partial\tilde{v}}{\partial x}\right)^2 + \left(\frac{\partial\tilde{w}}{\partial x}\right)^2\right], \tag{5a}$$

$$\varepsilon_\theta = \frac{1}{R+z}\left(\frac{\partial\tilde{v}}{\partial\theta} + \tilde{w}\right) + \frac{1}{2(R+z)^2}\left[\left(\frac{\partial\tilde{u}}{\partial\theta}\right)^2 + \left(\frac{\partial\tilde{v}}{\partial\theta} + \tilde{w}\right)^2 + \left(\frac{\partial\tilde{w}}{\partial\theta} - \tilde{v}\right)^2\right], \tag{5b}$$

$$\gamma_{x\theta} = \frac{\partial\tilde{v}}{\partial x} + \frac{1}{R+z}\frac{\partial\tilde{u}}{\partial\theta} + \frac{1}{R+z}\left[\frac{\partial\tilde{u}}{\partial x}\frac{\partial\tilde{u}}{\partial\theta} + \frac{\partial\tilde{v}}{\partial x}\left(\frac{\partial\tilde{v}}{\partial\theta} + \tilde{w}\right) + \frac{\partial\tilde{w}}{\partial x}\left(\frac{\partial\tilde{w}}{\partial\theta} - \tilde{v}\right)\right]. \tag{5c}$$

The thinness approximations are introduced such that

$$\frac{1}{R+z} = \frac{1}{R}\left[1 - \frac{z}{R} + O\left(\left(\frac{z}{R}\right)^2\right)\right], \quad \frac{1}{(R+z)^2} = \frac{1}{R^2}\left[1 - \frac{2z}{R} + O\left(\left(\frac{z}{R}\right)^2\right)\right], \tag{6a, b}$$

where $O((z/R)^2)$ is a small quantity of order $(z/R)^2$. Eqs. (5) coincide with those obtained by Novozhilov [30], who did not consider geometric imperfections and neglected z and z^2 at this point of the derivation with respect to R. By introducing Eqs. (4) into Eqs. (5) and using approximations (6), the middle surface strain–displacement relationships, changes in the curvature and torsion are obtained for the Flügge–Lur'e-Byrne non-linear shell theory [21,28]

$$\varepsilon_{x,0} = \frac{\partial u}{\partial x} + \frac{1}{2}\left[\left(\frac{\partial u}{\partial x}\right)^2 + \left(\frac{\partial v}{\partial x}\right)^2 + \left(\frac{\partial w}{\partial x}\right)^2\right] + \frac{\partial w}{\partial x}\frac{\partial w_0}{\partial x} \tag{7a}$$

$$\varepsilon_{\theta,0} = \frac{\partial v}{R\partial\theta} + \frac{w}{R} + \frac{1}{2R^2}\left[\left(\frac{\partial u}{\partial\theta}\right)^2 + \left(\frac{\partial v}{\partial\theta} + w\right)^2 + \left(\frac{\partial w}{\partial\theta} - v\right)^2\right] + \frac{1}{R^2}\left[\frac{\partial w_0}{\partial\theta}\left(\frac{\partial w}{\partial\theta} - v\right) + w_0\left(w + \frac{\partial v}{\partial\theta}\right)\right], \tag{7b}$$

$$\gamma_{x\theta,0} = \frac{\partial v}{\partial x} + \frac{\partial u}{R\partial\theta} + \frac{1}{R}\left[\frac{\partial u}{\partial x}\frac{\partial u}{\partial\theta} + \frac{\partial v}{\partial x}\left(\frac{\partial v}{\partial\theta} + w\right) + \frac{\partial w}{\partial x}\left(\frac{\partial w}{\partial\theta} - v\right) + \frac{\partial w_0}{\partial x}\left(\frac{\partial w}{\partial\theta} - v\right) + \frac{\partial w}{\partial x}\frac{\partial w_0}{\partial\theta} + \frac{\partial v}{\partial x}w_0\right]. \tag{7c}$$

$$k_x = -\frac{\partial^2 w}{\partial x^2} - \frac{\partial u}{\partial x}\frac{\partial^2(w+w_0)}{\partial x^2} - \frac{\partial v}{\partial x}\frac{\partial^2(w+w_0)}{R\partial x\partial\theta} + \frac{1}{R}\left(\frac{\partial v}{\partial x}\right)^2 \tag{7d}$$

$$k_\theta = -\frac{\partial^2 w}{R^2\partial\theta^2} - \frac{w}{R^2} - \frac{(w+w_0)}{R^3}\left(w + \frac{\partial^2 w}{\partial\theta^2} + \frac{\partial v}{\partial\theta}\right) - \frac{w}{R^3}\left(w_0 + \frac{\partial^2 w_0}{\partial\theta^2}\right) - \frac{\partial u}{R^2\partial\theta}\left(\frac{\partial u}{R\partial\theta} + \frac{\partial^2(w+w_0)}{\partial x\partial\theta}\right) - \frac{\partial v}{R^3\partial\theta}\frac{\partial^2(w+w_0)}{\partial\theta^2}, \tag{7e}$$

$$k_{x\theta} = -2\frac{\partial^2 w}{R\partial x\partial\theta} + \frac{\partial v}{R\partial x} - \frac{\partial u}{R^2\partial\theta} - \frac{\partial u}{R\partial x}\left(\frac{\partial u}{R\partial\theta} + \frac{\partial^2(w+w_0)}{\partial x\partial\theta}\right) + \frac{\partial v}{R^2\partial x}\left(\frac{\partial v}{\partial\theta} - \frac{\partial^2(w+w_0)}{\partial\theta^2}\right) - \frac{\partial^2(w+w_0)}{R^2\partial x\partial\theta}\left(w + \frac{\partial v}{\partial\theta}\right) - \frac{\partial^2 w}{R^2\partial x\partial\theta}w_0 - \frac{\partial^2(w+w_0)}{\partial x^2}\frac{\partial u}{R\partial\theta} - \frac{\partial v}{\partial x}\frac{\partial^2(w+w_0)}{R^2\partial\theta^2}. \tag{7f}$$

It is important to note that, in contrast to Refs. [21,28], non-linear terms in changes in curvature and torsion are retained in Eqs. (7d–f). Eqs. (7) have been obtained by neglecting higher order terms in z, in order to reduce Eqs. (5) to the form given by Eqs. (1). Eq. (7a)–(7c) coincide with those obtained by Novozhilov [30], excluding geometric imperfections that were not considered in Ref. [30].

According to Novozhilov's non-linear shell theory, Eqs. (4) are replaced by [30]

$$\tilde{u} = u + z\theta, \quad \tilde{v} = v + z\psi, \quad \tilde{w} = w + w_0 + z\chi, \tag{8a–c}$$

where

$$\theta = -\frac{\partial(w+w_0)}{\partial x}\left(1 + \frac{\partial v}{R\partial\theta} + \frac{w}{R}\right) + \left(\frac{\partial(w+w_0)}{R\partial\,\theta} - \frac{v}{R}\right)\frac{\partial u}{R\partial\theta} - \frac{\partial w}{\partial x}\frac{w_0}{R} \tag{8d}$$

$$\psi = -\left(\frac{\partial(w+w_0)}{R\partial\theta} - \frac{v}{R}\right)\left(1 + \frac{\partial u}{\partial x}\right) + \frac{\partial(w+w_0)}{\partial x}\frac{\partial v}{\partial x}, \tag{8e}$$

$$\chi \cong \frac{\partial u}{\partial x} + \frac{\partial v}{R\partial\theta} + \frac{\partial u}{\partial x}\frac{\partial v}{R\partial\theta} - \frac{\partial u}{R\partial\theta}\frac{\partial v}{\partial x} \tag{8f}$$

Substituting Eqs. (4) and (6) into Eqs. (5), expressions for changes in the curvature and torsion are obtained as

$$k_x = -\frac{\partial^2 w}{\partial x^2} + \frac{\partial v}{R\partial x}\left(\frac{\partial u}{R\partial\theta} + \frac{\partial v}{\partial x} - \frac{\partial^2(w+w_0)}{\partial x\partial\theta}\right) + \frac{\partial(w+w_0)}{\partial x}\left(\frac{\partial^2 u}{\partial x^2} - \frac{\partial w}{R\partial x}\right) - \frac{\partial w}{\partial x}\frac{\partial w_0}{R\partial x} + \frac{\partial^2 u}{R\partial x\partial\theta}\left(\frac{v}{R} - \frac{\partial(w+w_0)}{R\partial\theta}\right) - \frac{\partial^2(w+w_0)}{R\partial x\partial\theta}\frac{\partial u}{R\partial\theta} - \frac{\partial^2(w+w_0)}{\partial\, x^2}\left(\frac{w}{R} + \frac{\partial v}{R\partial\theta} + \frac{\partial u}{\partial x}\right) - \frac{\partial^2 w}{\partial x^2}\frac{w_0}{R}, \tag{9a}$$

$$k_\theta = -\frac{\partial^2 w}{R^2\partial\theta^2} - \frac{w}{R^2} + \frac{\partial u}{R\partial x} + \frac{\partial v}{R^2\partial\theta} - \frac{(w+w_0)}{R^2}\left(\frac{w}{R} + \frac{\partial^2 w}{R\partial\theta^2} - \frac{\partial u}{\partial x}\right) - \frac{w}{R^3}\left(w_0 t\frac{\partial^2 w_0}{\partial\theta^2}\right) - \frac{\partial u}{R^2\partial\theta}\left(\frac{\partial u}{R\partial\theta}\frac{\partial v}{\partial x} + \frac{\partial^2(w+w_0)}{\partial x\partial\theta}\right) + \frac{\partial v}{R^2\partial\theta}\left(\frac{\partial v}{R\partial\theta} - \frac{\partial^2(w+w_0)}{R\partial\theta^2} + 3\frac{\partial u}{\partial x}\right) + \frac{\partial^2 v}{R\partial\theta^2}\left(\frac{\partial(w+w_0)}{R^2\partial\theta} + \frac{v}{R^2}\right) - \frac{\partial^2(w+w_0)}{R^2\partial\theta^2}\frac{\partial u}{\partial x} - \frac{\partial(w+w_0)}{R\partial x}\frac{\partial^2 v}{\partial x\partial\theta} - \frac{\partial v}{R\partial x}\frac{\partial^2(w+w_0)}{\partial x\partial\theta}, \tag{9b}$$

$$k_{x\theta} = -2\frac{\partial^2 w}{R\partial x\partial\theta} + \frac{\partial v}{R\partial x} - \frac{\partial u}{R^2\partial\theta} - \frac{\partial u}{R^2\partial\theta}\left(\frac{\partial u}{\partial x} + \frac{\partial^2(w+w_0)}{\partial\theta^2} - \frac{\partial v}{R\partial\theta}\right) - \frac{\partial^2(w+w_0)}{\partial x^2}\left(\frac{\partial u}{R\partial\theta} + \frac{\partial v}{\partial x}\right) + \frac{\partial v}{R\partial x}\left(2\frac{\partial v}{R\partial\theta} - \frac{\partial^2(w+w_0)}{R\partial\theta^2} + 2\frac{\partial u}{\partial x}\right) - 2\frac{\partial^2(w+w_0)}{R\partial x\partial\theta}\left(\frac{w}{R} + \frac{\partial v}{R\partial\theta} + \frac{\partial u}{\partial x}\right) - 2\frac{\partial^2 w}{R^2\partial x\partial\theta}w_0 + \frac{v}{R^2}\left(\frac{\partial^2 u}{R\partial\theta^2} - \frac{\partial^2 v}{\partial x\partial\theta}\right) - \frac{\partial(w+w_0)}{R^2\partial\theta}\left(\frac{\partial^2 u}{R\partial\theta^2} - \frac{\partial w}{\partial x} + \frac{\partial^2 v}{\partial x\partial\theta}\right) + \frac{\partial w}{R^2\partial\theta}\frac{\partial w_0}{\partial x} + \frac{\partial(w+w_0)}{\partial x}\left(\frac{\partial^2 u}{R\partial x\partial\theta} - \frac{\partial^2 v}{\partial x^2}\right). \tag{9c}$$

The middle surface strain–displacement relationships are still given by Eqs. (7a)–(7c). Eqs. (7a)–(7c) and (9a)–(9c) together are an improved version of the Novozhilov's non-linear shell theory because approximations (6) have been used instead of neglecting terms in z and z^2 at this point of the derivation as done in Ref. [30].

The elastic strain energy U_S of a circular cylindrical shell, neglecting σ_z as stated by Love's first approximation assumptions, is given by Ref. [33]

$$U_S = \frac{1}{2}\int_0^{2\pi}\int_0^{L}\int_{-h/2}^{h/2}(\sigma_x\varepsilon_x + \sigma_\theta\varepsilon_\theta + \tau_{x\theta}\,\gamma_{x\theta})\,\mathrm{d}x\,R(1+z/R)\mathrm{d}\theta\,\mathrm{d}z, \tag{10}$$

where h is the shell thickness, R is the shell middle radius, L is the shell length and the stresses σ_x, σ_θ and $\tau_{x\theta}$ are related to the strain for homogeneous and isotropic material ($\sigma_z = 0$, case of plane stress) by Ref. [33]

$$\sigma_x = \frac{E}{1-\nu^2}(\varepsilon_x + \nu\varepsilon_\theta) \quad \sigma_\theta = \frac{E}{1-\nu^2}(\varepsilon_\theta + \nu\varepsilon_x) \quad \tau_{x\theta} = \frac{E}{2(1+\nu)}\gamma_{x\theta} \tag{11a–c}$$

where E is Young's modulus and v is the Poisson ratio. By using Eqs. (1), (10) and (11), the following expression is obtained

$$U_S = \frac{1}{2}\frac{Eh}{1-v^2}\int_0^{2\pi}\int_0^L \left(\varepsilon_{x,0}^2 + \varepsilon_{\theta,0}^2 + 2v\varepsilon_{x,0}\varepsilon_{\theta,0} + \frac{1-v}{2}\gamma_{x\theta,0}^2\right) \mathrm{d}\,xR\,\mathrm{d}\,\theta + \frac{1}{2}\frac{Eh^3}{12(1-v^2)}\int_0^{2\pi}\int_0^L \left(k_x^2 + k_\theta^2 + 2vk_xk_\theta + \frac{1-v}{2}k_{x\theta}^2\right) \mathrm{d}\,x\;R\,\mathrm{d}\,\theta + \frac{1}{2}\frac{Eh^3}{6R(1-v^2)}\int_0^{2\pi}\int_0^L \left(\varepsilon_{x,0}k_x + \varepsilon_{\theta,0}k_\theta + v\varepsilon_{x,0}k_\theta + v\varepsilon_{\theta,0}\;k_x + \frac{1-v}{2}\gamma_{x\theta,0}k_{x\theta}\right) \mathrm{d}\,x\;R\,\mathrm{d}\,\theta + O(h^4), \tag{12}$$

where $O(h^4)$ is a higher order term in h and the last term disappears if z/R is neglected with respect to unity in Eq. (10), as it must be for Donnell's and Sanders–Koiter theories. If this term is neglected, the right side of Eq. (12) can be easily interpreted: the first term is the membrane (also referred to as stretching) energy and the second one is the bending energy. If the last term is retained, membrane and bending energies are coupled. In the appendix, the expressions of the strain energy for orthotropic and symmetric cross-ply laminated composite shells are reported.

3. Mode expansion, kinetic energy and external loads

The kinetic energy T_S of a circular cylindrical shell, by neglecting rotary inertia, is given by

$$T_S = \frac{1}{2}\rho_S h\int_0^{2\pi}\int_0^L \left(\dot{u}^2 + \dot{v}^2 + \dot{w}^2\right) \mathrm{d}x\;R\;\mathrm{d}\theta \tag{13}$$

where ρ_S is the mass density of the shell. In Eq. (13) the overdot denotes a time derivative. The virtual work W done by the external forces is written as

$$W = \int_0^{2\pi}\int_0^L (q_x u + q_\theta v + q_r w)\,\mathrm{d}x\;R\;\mathrm{d}\theta, \tag{14}$$

where q_x, q_θ and q_r are the distributed forces per unit area acting in axial, circumferential and radial directions, respectively. Initially, only a single harmonic radial force is considered; therefore $q_x = q_\theta = 0$. The external radial distributed load q_r applied to the shell, due to the radial concentrated force $\tilde{f}$, is given by

$$q_r = \tilde{f}\delta(R\theta - R\tilde{\theta})\delta(x - \tilde{x})\cos(\omega t), \tag{15}$$

where ω is the excitation frequency, t is the time, δ is the Dirac delta function, $\tilde{f}$ gives the radial force amplitude positive in the z direction, $\tilde{x}$ and $\tilde{\theta}$ give the axial and angular positions of the point of application of the force, respectively; here, the point excitation is located at $\tilde{x} = L/2$, $\tilde{\theta} = 0$. Eq. (14) can be rewritten in the form

$$W = \tilde{f}\cos(\omega\,t)(w)_{x=L/2,\;\theta=0}. \tag{16}$$

Eq. (16) adapted particularly specialised for the expression of w used in the present study is given in Section 5, together with the virtual work of axial loads and uniform radial pressure.

In order to reduce the system to finite dimensions, the middle surface displacements u, v and w are expanded by using approximate functions. The following boundary conditions are imposed at the shell ends, $x = 0$, L:

$$w = w_0 = 0, \tag{17a}$$

$$M_x = 0 \tag{17b}$$

$$\partial^2 w_0/\partial x^2 = 0, \tag{17c}$$

$$N_x = 0, \tag{17d}$$

$$v = 0, \tag{17e}$$

where M_x is the bending moment per unit length and N_x is the axial force per unit length; moreover, u, v and w must be continuous in θ.

Past studies show that a linear modal base is the simplest choice to discretize the system. In particular, in order to reduce the number of degrees of freedom (d.o.f.), it is important to use only the most significant modes. It is necessary to consider, in addition to the asymmetric mode directly driven into vibration by the excitation given in Eq. (15) (driven modes), (i) the orthogonal mode having the same shape and natural frequency but rotated by $\pi/(2n)$ (companion modes), (ii) additional asymmetric modes, and (iii) axisymmetric modes. In fact, it has clearly been established that, for large-amplitude shell vibrations, the deformation of the shell involves significant axisymmetric oscillations inwards. According to these considerations, the displacements u, v and w are expanded by using the eigenmodes of the simply supported, empty shell (which are unchanged for the completely filled shell with open ends):

$$u(x,\theta,t) = \sum_{m=1}^{M_1}\sum_{j=1}^{N}\left[u_{m,j,c}(t)\cos(j\theta) + u_{m,j,s}(t)\sin(j\theta)\right]\cos(\lambda_m x) + \sum_{m=1}^{M_2} u_{m,0}(t)\cos(\lambda_m x), \tag{18a}$$

$$v(x,\theta,t) = \sum_{m=1}^{M_1}\sum_{j=1}^{N}\left[v_{m,j,c}(t)\sin(j\theta) + v_{m,j,s}(t)\cos(j\theta)\right]\sin(\lambda_m x) + \sum_{m=1}^{M_2} v_{m,0}(t)\sin(\lambda_m x), \tag{18b}$$

$$w(x,\theta,t) = \sum_{m=1}^{M_1}\sum_{j=1}^{N}\left[w_{m,j,c}(t)\cos(j\theta) + w_{m,j,s}(t)\sin(j\theta)\right]\sin(\lambda_m x) + \sum_{m=1}^{M_2} w_{m,0}(t)\sin(\lambda_m x), \tag{18c}$$

where j is the number of circumferential waves, m is the number of longitudinal half-waves, $\lambda_m = m\pi/L$ and t is the time; $u_{m,j}(t)$, $v_{m,j}(t)$ and $w_{m,j}(t)$ are the generalized co-ordinates that are unknown functions of t; the additional subscript c or s indicates if the generalized coordinate is associated to a cos or sin function in θ except for v, for which the notation is reversed (no additional subscript is used for axisymmetric terms). The integers N, M_1 and M_2 must be selected with care in order to obtain the required accuracy and acceptable dimension of the non-linear problem.

Excitation in the neighbourhood of resonance of mode with $m = 1$ longitudinal half-wave and n circumferential waves, indicated as resonant mode (m, n) for simplicity, is considered. The minimum number of d.o.f. that has been found to be necessary to predict the non-linear response

with good accuracy is 14. It is observed, for symmetry reasons, that the non-linear interaction among linear modes of the chosen base involves the asymmetric modes ($n>0$) having a given n value (e.g., the resonant mode), the asymmetric modes having a multiple of this value of circumferential waves ($k\times n$, where k is an integer), and axisymmetric modes ($n=0$); asymmetric modes with different numbers of circumferential waves, that do not satisfy the relationship $k\times n$, have interaction only if their natural frequencies are very close to relationship 1:1, 1:2 or 1:3 with the frequency of the resonant mode. Only modes with an odd m value of longitudinal half-waves can be considered for symmetry reasons [8–10] (if geometric imperfections with an even m value are not introduced). In particular, asymmetric modes having up to three longitudinal half-waves ($M_1=3$, only odd m values) and modes having n, $2\times n$, $3\times n$ and $4\times n$ circumferential waves have been considered in the numerical calculations. For axisymmetric modes, up to $M_2=9$ has been used (only odd m values).

The minimal expansion used in the numerical calculation (see Section 6) for excitation in the neighbourhood of resonance of mode ($m=1$, n) is

$$u(x,\theta,t)=\left[u_{1,n,c}(t)\cos(n\theta)+u_{1,n,s}(t)\sin(n\theta)\right]\cos(\lambda_1 x)+\sum_{m=1}^{2}u_{2m-1,0}(t)\cos(\lambda_{2m-1}x), \tag{19a}$$

$$\begin{aligned}v(x,\theta,t)=&\sum_{k=1}^{2}\left[v_{1,kn,c}(t)\sin(kn\theta)+v_{1,kn,s}(t)\cos(kn\theta)\right]\sin(\lambda_1 x)\\&+\left[v_{3,2n,c}(t)\sin(2n\theta)+v_{3,2n,s}(t)\cos(2n\theta)\right]\sin(\lambda_3 x),\end{aligned} \tag{19b}$$

$$w(x,\theta,t)=\left[w_{1,n,c}(t)\cos(n\theta)+w_{1,n,s}(t)\sin(n\theta)\right]\sin(\lambda_1 x)+\sum_{m=1}^{2}w_{2m-1,0}(t)\sin(\lambda_{2m-1}x). \tag{19c}$$

This expansion has 14 generalized co-ordinates (d.o.f.) and guarantees good accuracy for the calculation performed in the present work. Accuracy and convergence of the solution have been checked numerically (see Section 6). It has been verified that no terms can be eliminated from the expansion given in Eqs. (19) without introducing large errors in the shell response. However, in most of calculations 16 or more (26, 36 and 48) generalized co-ordinates have been used. In the expansion with 16 co-ordinates, which has been largely used, terms $\left[u_{1,2n,c}(t)\cos(2n\theta)+u_{1,2n,s}(t)\sin(2n\theta)\right]\cos(\lambda_1 x)$ have been added to Eq. (19a); however, they do not give a significant improvement to the accuracy of the solution with respect to Eqs. (19) (see Section 6). It can be observed that, if a different choice for the mode expansion with respect to Eq. (18) is used, a different number of generalized coordinates is necessary to obtain good accuracy.

The point excitation considered in Eq. (15) gives a non-zero contribution only to modes described by a cos function in an angular direction, referred to as the driven modes, and to axisymmetric modes. The modes having the shape of the driven modes, but rotated by $\pi/(2n)$, i.e., with form described by sin function in angular direction θ, are referred to as the companion mode.

It is extremely interesting to observe that in Eqs. (19a) and (19c) only the resonant driven and companion modes plus the first and third axisymmetric modes are retained in the minimal expansion. This is in perfect agreement with the result obtained in Refs. [8,9,34] for the expansion of the radial displacement w used with Donnell's non-linear shallow-shell theory. For the

circumferential displacement v, no axisymmetric modes are necessary. In fact, the first axisymmetric modes with radial displacement have axial displacement but zero circumferential displacement. However, it is necessary to retain in the expansion of v terms with $2n$ circumferential waves and three longitudinal half-waves. It must be clarified that Donnell's non-linear shallow-shell theory takes into account in-plane displacements by using the stress function, which has terms having twice the axial and angular wavenumbers of radial terms [8–10].

3.1. Travelling wave response

The presence of couples of modes having the same shape but different angular orientations, the first one described by $\cos(n\theta)$ (driven mode for the excitation given by Eq. (15)) and the other by $\sin(n\theta)$ (companion mode), in the periodic response of the shell leads to the appearance of travelling-wave vibration around the shell in the angular direction. This phenomenon is related to the axial symmetry of the system and is a fundamental difference vis-à-vis linear vibrations.

Away from resonance, the companion mode solution disappears ($u_{m,n,s}(t) = v_{m,n,s}(t) = w_{m,n,s}(t) = 0$) and the generalized co-ordinates are nearly in phase or in opposite phase. The presence of the companion mode in the shell response leads to the appearance of a travelling wave and to more complex phase-relationships among the generalized co-ordinates. The mode shapes are represented by Eq. (19). Let we consider for simplicity only radial motion, which is predominant for shells not particularly long. Supposing that the response of the driven and companion modes have the same frequency of oscillation of the excitation, i.e., $w_{1,n,c}(t) = \bar{w}_{1,n,c}\cos(\omega t + \theta_1)$ and $w_{1,n,s}(t) = \bar{w}_{1,n,s}\cos(\omega t + \theta_2)$, and considering the other co-ordinates having smaller amplitude, Eq. (19c) can be rearranged as

$$w = \big\{\big[\bar{w}_{1,n,c}\cos(\omega t + \theta_1) + \bar{w}_{1,n,s}\sin(\omega t + \theta_2)\big]\cos(n\theta) + \bar{w}_{1,n,s}\sin(n\theta - \omega t - \theta_2)\big\}\sin(\pi x/L) + O(\bar{w}^2_{1,n,c}, \bar{w}^2_{1,n,s}, \bar{w}_{1,0}, \bar{w}_{3,0}, \cdots)\,, \tag{20}$$

where $\bar{w}_{1,n,c}$ and $\bar{w}_{1,n,s}$ are the amplitudes of driven and companion modes, respectively, θ_1 and θ_2 are the phases and O is a small quantity. Eq. (20) gives a combined solution consisting of a standing wave and a travelling wave of amplitude $\bar{w}_{1,n,s}$ and moving in angular direction around the shell with angular velocity ω/n. The resulting standing wave is given by the sum of the two standing waves, one of amplitude $\bar{w}_{1,n,c}$ and the second of amplitude $\bar{w}_{1,n,s}$, having the same circular frequency ω and the same shape, but having a phase difference of $\theta_2 - \theta_1 - \pi/2$. When $\theta_2 - \theta_1 \cong \pi/2$, as it is generally observed in calculations and experiments, the amplitude of the resulting standing wave is almost $\bar{w}_{1,n,c} - \bar{w}_{1,n,s}$. In case of zero phase difference, i.e., $\theta_2 - \theta_1 = 0$, no travelling wave arises.

3.2. Geometric imperfections

Initial geometric imperfections of the circular cylindrical shell are considered only in radial direction. They are associated with zero initial stress. The radial imperfection w_0 is expanded in the same form of w, i.e., in a double Fourier series satisfying the boundary conditions (17a), (17c)

at the shell edges

$$w_0(x,\theta)=\sum_{m=1}^{\tilde{M}_1}\sum_{n=1}^{\tilde{N}}\left[A_{m,n}\cos(n\theta)+B_{m,n}\sin(n\theta)\right]\sin(\lambda_m x)+\sum_{m=1}^{\tilde{M}_2}A_{m,0}\sin(\lambda_m x)\,, \tag{21}$$

where $A_{m,n}$, $B_{m,n}$ and $A_{m,0}$ are the modal amplitudes of imperfections; $\tilde{N}$, $\tilde{M}_1$ and $\tilde{M}_2$ are integers indicating the number of terms in the expansion.

3.3. Boundary conditions

Eq. (17) give the boundary conditions for a simply supported shell. Eqs. (17a), (17c) and (17e) are identically satisfied by the expansions of u, v, w and w_0. Moreover, the continuity in θ of all the displacement is also satisfied. On the other hand, Eqs. (17b) and (17d) can be rewritten in the form [33]

$$M_x=\frac{Eh^3}{12(1-\nu^2)}(k_x+\nu k_\theta)=0, \tag{22}$$

$$N_x=\frac{Eh}{1-\nu^2}\left(\varepsilon_{x,0}+\nu\varepsilon_{\theta,0}\right)=0. \tag{23}$$

Eq. (22) is identically satisfied for the expressions of k_x and k_θ given in Eqs. (2d), (2e) and (3d), (3e) for Donnell's and Sanders–Koiter non-linear shell theories, respectively. For Flügge–Lur'e-Byrne, modified in order to retain non-linear terms in changes of curvature and torsion, and Novozhilov's non-linear shell theories, Eq. (22) is not satisfied only by non-linear terms that are extremely small for thin shells; for this reason, Eq. (22) can be considered identically satisfied also for these two shell theories.

Eq. (23) is not identically satisfied for any of the non-linear shell theories. According to Sanders–Koiter theory, see Eqs. (3a),(3b), and eliminating null terms at the shell edges, Eq. (23) can be rewritten as

$$\left[\frac{\partial\hat{u}}{\partial x}+\frac{1}{8}(1+\nu)\left(\frac{\partial v}{\partial x}-\frac{\partial u}{R\partial\theta}\right)^2+\frac{1}{2}\left(\frac{\partial w}{\partial x}\right)^2+\frac{\partial w}{\partial x}\frac{\partial w_0}{\partial x}\right]_{x=0,L}=0, \tag{24}$$

where $\hat{u}$ is a term added to the expansion of u, given in Eq. (18a) and (19a), in order to satisfy exactly the axial boundary conditions $N_x=0$ ($\partial u/\partial x=0$ at $x=0$, L according to Eqs. (18a) and (19a)). As a consequence that $\hat{u}$ is a second-order term in the shell displacement, it has not been inserted in the second-order terms that involve u in Eq. (24).

All the generalized co-ordinates, except the six associated with the resonant mode (m, n), which are $u_{m,n,c}(t)$, $v_{m,n,c}(t)$, $w_{m,n,c}(t)$, $u_{m,n,s}(t)$, $v_{m,n,s}(t)$, $w_{m,n,s}(t)$, are neglected because they are an infinitesimal of higher order. Calculations give

$$\begin{aligned}\hat{u}(t)=&-\tfrac{1}{32}[a(t)+b(t)\cos(2n\theta)+c(t)\sin(2n\theta)]\sin(2m\pi x/L)-(m\pi/L)\\&\times\left[w_{m,n,c}(t)\cos(n\,\theta)+w_{m,n,s}(t)\sin(n\theta)\right]\sum_{j=0}^{\tilde{N}}\sum_{i=1}^{\tilde{M}}\frac{i}{m+i}\left[A_{m,n}\cos(j\theta)+B_{m,n}\sin(j\theta)\right]\\&\times\sin\left[(m+i)\pi x/L\right],\end{aligned} \tag{25}$$

where $\tilde{M}$ is the largest between $\tilde{M}_1$ and $\tilde{M}_2$ and

$$a(t) = (4m\pi/L)\left(w_{m,n,c}^2 + w_{m,n,s}^2\right) + (1+\nu)(m\pi/L)\left(v_{m,n,c}^2 + v_{m,n,s}^2\right) + (1+\nu)\left[Ln^2/(m\pi R^2)\right]\left(u_{m,n,c}^2 + u_{m,n,s}^2\right) - 2(1+\nu)(n/R)\left(v_{m,n,s}u_{m,n,s} - v_{m,n,c}u_{m,n,c}\right), \quad (26)$$

$$b(t) = (4m\pi/L)\left(w_{m,n,c}^2 - w_{m,n,s}^2\right) + (1+\nu)(m\pi/L)\left(v_{m,n,s}^2 - v_{m,n,c}^2\right) + (1+\nu)\left[Ln^2/(m\pi R^2)\right]\left(u_{m,n,s}^2 - u_{m,n,c}^2\right) - 2(1+\nu)(n/R)\left(v_{m,n,s}u_{m,n,s} + v_{m,n,c}u_{m,n,c}\right), \quad (27)$$

$$c(t) = (8m\pi/L)w_{m,n,c}w_{m,n,s} + 2(1+\nu)(m\pi/L)v_{m,n,c}v_{m,n,s} - 2(1+\nu)\left[Ln^2/(m\pi R^2)\right]u_{m,n,c}u_{m,n,s} - 2(1+\nu)(n/R)\left(v_{m,n,c}u_{m,n,s} - v_{m,n,s}u_{m,n,c}\right). \quad (28)$$

For Donnell's, Flügge–Lur'e-Byrne and Novozhilov's non-linear shell theories, Eq. (25) is still correct, but Eqs. (26–28) are simplified. For Donnell's non-linear shell theory

$$a(t) = (4m\pi/L)\left(w_{m,n,c}^2 + w_{m,n,s}^2\right), \quad b(t) = (4m\pi/L)\left(w_{m,n,c}^2 - w_{m,n,s}^2\right), \quad c(t) = (8m\pi/L)w_{m,n,c}w_{m,n,s}. \quad (29-31)$$

For Flügge–Lur'e-Byrne and Novozhilov's theories

$$a(t) = (4m\pi/L)\left(w_{m,n,c}^2 + w_{m,n,s}^2 + v_{m,n,c}^2 + v_{m,n,s}^2\right) + 4\nu\left[Ln^2/(m\pi R^2)\right]\left(u_{m,n,c}^2 + u_{m,n,s}^2\right), \quad (32)$$

$$b(t) = (4m\pi/L)\left(w_{m,n,c}^2 - w_{m,n,s}^2 + v_{m,n,s}^2 - v_{m,n,c}^2\right) + 4\nu\left[Ln^2/(m\pi R^2)\right]\left(u_{m,n,s}^2 - u_{m,n,c}^2\right), \quad (33)$$

$$c(t) = (8m\pi/L)\left(w_{m,n,c}w_{m,n,s} + v_{m,n,c}v_{m,n,s}\right) - 8\nu\left[Ln^2/(m\pi R^2)\right]u_{m,n,c}u_{m,n,s}. \quad (34)$$

4. Fluid–structure interaction

The contained fluid is assumed to be incompressible and inviscid; these hypotheses turned out to be adequate for vibrations of water-filled shells [10]. The shell prestress due to the fluid weight is neglected; in the cases numerically investigated this prestress is extremely small. The non-linear effects in the dynamic pressure and in the boundary conditions at the fluid–structure interface are also neglected. These non-linear effects have been found to be negligible by Gonçalves and Batista [17] and Lakis and Laveau [35]; in fact, the amplitude of shell displacements remains small enough for linear fluid mechanics to be adequate. The fluid motion is described by the velocity potential $\mathbf{\Phi}$, which satisfies the Laplace equation,

$$\nabla^2\mathbf{\Phi} = \frac{\partial^2\mathbf{\Phi}}{\partial x^2} + \frac{\partial^2\mathbf{\Phi}}{\partial r^2} + \frac{1}{r}\frac{\partial\mathbf{\Phi}}{\partial r} + \frac{1}{r^2}\frac{\partial^2\mathbf{\Phi}}{\partial\theta^2} = 0. \quad (35)$$

The fluid velocity vector $\mathbf{v}$ is related to $\mathbf{\Phi}$ by $\mathbf{v} = -\nabla\mathbf{\Phi}$. No cavitation is assumed at the fluid-shell interface,

$$\left(\partial\mathbf{\Phi}/\partial r\right)_{r=R} = -\dot{w}. \quad (36)$$

Both ends of the fluid volume (in correspondence to the shell edges) are assumed to be open, so that a zero pressure is assumed there,

$$(\mathbf{\Phi})_{x=0} = (\mathbf{\Phi})_{x=L} = 0. \tag{37}$$

A solution of Eq. (35) satisfying condition (36) is given by

$$\mathbf{\Phi} = \sum_{m=1}^{\infty}\sum_{n=0}^{\infty}\left[\alpha_{mn}(t)\cos(n\theta) + \beta_{mn}(t)\sin(n\theta)\right]\left[c_{mn}\mathrm{I}_n(\lambda_m r) + d_{mn}\mathrm{K}_n(\lambda_m r)\right]\sin(\lambda_m x), \tag{38}$$

where $\mathrm{I}_n(r)$ and $\mathrm{K}_n(r)$ are the modified Bessel functions of the first and second kind, respectively, of order n and $\lambda_m = m\pi/L$. Eq. (38) must satisfy boundary condition (36) and $\mathbf{\Phi}$ must be finite (regular) at $r = 0$. By using the assumed mode expansion of w, given by Eq. (18c), the solution of the boundary-value problem for internal fluid only is

$$\mathbf{\Phi} = -\sum_{m=1}^{M}\sum_{n=0}^{N}\left[\dot{w}_{m,n,c}(t)\cos(n\theta) + \dot{w}_{m,n,s}(t)\sin(n\theta)\right]\frac{\mathrm{I}_n(\lambda_m r)}{\lambda_m \mathrm{I}'_n(\lambda_m R)}\sin(\lambda_m x), \tag{39}$$

where $\mathrm{I}'_n(r)$ is the derivative of $\mathrm{I}_n(r)$ with respect to its argument and M is the largest between M_1 and M_2, which have been introduced in Eq. (18). Axisymmetric generalized co-ordinates are included with the subscript c for brevity. Therefore, the dynamic pressure p exerted by the contained fluid on the shell is given by

$$p = \rho_F\left(\dot{\mathbf{\Phi}}\right)_{r=R} = -\rho_F\sum_{m=1}^{M}\sum_{n=0}^{N}\left[\ddot{w}_{m,n,c}(t)\cos(n\theta) + \ddot{w}_{m,n,s}(t)\sin(n\theta)\right]\frac{\mathrm{I}_n(\lambda_m R)}{\lambda_m \mathrm{I}'_n(\lambda_m R)}\sin(\lambda_m x), \tag{40}$$

where ρ_F is the mass density of the internal fluid. Eq. (40) shows that the fluid has an inertial effect on radial motion of the shell. In particular, the inertial effects are different for the asymmetric and the axisymmetric terms of the mode expansion. Hence, the fluid is expected to change the non-linear behaviour of the fluid-filled shell. Usually the inertial effect of the fluid is larger for axisymmetric modes, thus enhancing the non-linear behaviour of the shell.

Only kinetic energy T_F is associated to inviscid fluid without flow; by using the Green's theorem, this is given by

$$T_F = \frac{1}{2}\rho_F\int_0^{2\pi}\int_0^{L}(\mathbf{\Phi})_{r=R}\dot{w}\,\mathrm{d}x R\,\mathrm{d}\theta. \tag{41}$$

5. Lagrange equations of motion

The non-conservative damping forces are assumed to be of viscous type and are taken into account by using the Rayleigh's dissipation function

$$F = \frac{1}{2}c\int_0^{2\pi}\int_0^{L}\left(\dot{u}^2 + \dot{v}^2 + \dot{w}^2\right)\mathrm{d}x R\,\mathrm{d}\theta, \tag{42}$$

where c has a different value for each term of the mode expansion. Simple calculations give

$$F = \frac{1}{2}(L/2)R\sum_{n=0}^{N}\sum_{m=1}^{M}\psi_n\left[c_{m,n,c}(\dot{u}_{m,n,c}^2 + \dot{v}_{m,n,c}^2 + \dot{w}_{m,n,c}^2) + c_{m,n,s}(\dot{u}_{m,n,s}^2 + \dot{v}_{m,n,s}^2 + \dot{w}_{m,n,s}^2)\right], \quad (43)$$

where

$$\psi_n = \begin{cases} 2\pi & \text{if } n = 0, \\ \pi & \text{if } n > 0. \end{cases} \quad (44)$$

The damping coefficient $c_{m,n,c \text{ or } s}$ is related to modal damping ratio, that can be evaluated from experiments, by $\varsigma_{m,n,c \text{ or } s} = c_{m,n,c \text{ or } s}/(2\mu_{m,n}\omega_{m,n})$, where $\omega_{m,n}$ is the natural circular frequency of mode (m, n) and $\mu_{m,n}$ is the modal mass of this mode, given by $\mu_{m,n} = \psi_n(\rho_S + \rho_V)h(L/2)R$, and the virtual mass due to contained fluid is

$$\rho_V = \frac{\rho_F}{\lambda_m h}\frac{\mathrm{I}_n(\lambda_m R)}{\mathrm{I}_n'(\lambda_m R)}. \quad (45)$$

The total kinetic energy of the system is

$$T = T_S + T_F. \quad (46)$$

The potential energy of the system is only the elastic strain energy of the shell

$$U = U_S. \quad (47)$$

The virtual work done by the concentrated radial force $\tilde{f}$, given by Eq. (16), is specialized for the expression of w given in

$$W = \tilde{f}\cos(\omega t)(w)_{x=L/2,\theta=0} = \tilde{f}\cos(\omega t)\left[\sum_{m=1}^{M_1}\sum_{j=1}^{N} w_{m,j,c}(t) + \sum_{m=1}^{M_2} w_{m,0}(t)\right]. \quad (48)$$

In presence of axial loads and radial pressure acting on the shell, additional virtual work is done by the external forces. Let we consider a time-dependent axial load $N(t)$ applied at both the shell ends; $N(t)$ is positive in the x direction. In particular $-N(t)$ is applied at $x = 0$ and $N(t)$ is applied at $x = L$. The axial distributed force q_x has the following expression:

$$q_x = N(t)[-\delta(x) + \delta(x - L)], \quad (49)$$

where $\boldsymbol{\delta}$ is the Dirac delta function. The virtual work done by the axial load is

$$\begin{aligned} W &= \int_0^{2\pi}\int_0^{L} N(t)[-\delta(x) + \delta(x - L)]u \,\mathrm{d}\, x R \,\mathrm{d}\, \theta \\ &= -4\pi R N(t)\sum_{m=1}^{M_2} u_{m,0}(t). \end{aligned} \quad (50)$$

In case of uniform internal time-varying pressure $p_r(t)$, the radial distributed force q_r is obviously

$$q_r = p_r(t). \quad (51)$$

The virtual work done by radial pressure is

$$W = \int_0^{2\pi} \int_0^L p_r(t) w \, \mathrm{d}\, x R \, \mathrm{d}\, \theta = 4Rp_r(t)L \sum_{m=1}^{M_2} w_{m,0}(t)/m. \tag{52}$$

Eqs. (50) and (52) show that only axisymmetric vibrations are directly excited by uniform axial loads and radial pressure.

The following notation is introduced for brevity:

$$\mathbf{q} = \left\{u_{m,n,c}, u_{m,n,s}, v_{m,n,c}, v_{m,n,s}, w_{m,n,c}, w_{m,n,s}\right\} \quad m = 1, \cdots M \text{ and } n = 0, \cdots N. \tag{53}$$

The generic element of the time-dependent vector $\mathbf{q}$ is referred to as q_j; the dimension of $\mathbf{q}$ is d.o.f., which is the number of d.o.f. used in the mode expansion.

The generalized forces Q_j are obtained by differentiation of the Rayleigh's dissipation function and of the virtual work done by external forces

$$Q_j = -\frac{\partial F}{\partial \dot{q}_j} + \frac{\partial W}{\partial q_j} = -c_{m,n,i,j,c/s}\dot{q}_j + \begin{cases} 0 & \text{if } q_j = u_{m,n,c/s}, v_{m,n,c/s} \text{ or } w_{m,n,s}, \\ \tilde{f}\cos(\omega t) & \text{if } q_j = w_{m,n,c}, \end{cases} \tag{54}$$

where the subscript c/s indicates c or s.

The Lagrange equations of motion for the fluid-filled shell are

$$\frac{\mathrm{d}}{\mathrm{d}t}\left(\frac{\partial T}{\partial \dot{q}_j}\right) - \frac{\partial T}{\partial q_j} + \frac{\partial U}{\partial q_j} = Q_j, \quad j = 1, \cdots \text{d.o.f.}, \tag{55}$$

where $\partial T/\partial q_j = 0$. These second order equations have very long expressions containing quadratic and cubic non-linear terms. In particular,

$$\frac{\mathrm{d}}{\mathrm{d}t}\left(\frac{\partial T}{\partial \dot{q}_j}\right) = \begin{cases} \rho_S h(L/2)\psi_n R\ddot{q}_j & \text{if } q_j = u_{m,n,c/s} \text{ or } v_{m,n,c/s}, \\ (\rho_S + \rho_V)h(L/2)\psi_n R\ddot{q}_j & \text{if } q_j = w_{m,n,c/s}, \end{cases} \tag{56}$$

which shows that no inertial coupling among the Lagrange equations exists for the shell with simply supported edges with the mode expansion used.

The very complicated term giving quadratic and cubic non-linearities can be written in the form

$$\frac{\partial U}{\partial q_j} = \sum_{k=1}^{\text{d.o.f.}} q_k f_k + \sum_{i,k=1}^{\text{d.o.f.}} q_i q_k f_{i,k} + \sum_{i,k,l=1}^{\text{d.o.f.}} q_i q_k q_l f_{i,k,l}, \tag{57}$$

where coefficients f have long expressions that include also geometric imperfections.

6. Numerical results

The equations of motion have been obtained by using the *Mathematica* 4 computer software [36] in order to perform analytical surface integrals of trigonometric functions. The generic Lagrange equation j is divided by the modal mass associated with $\ddot{q}_j$ and then is transformed in two first order equations. A non-dimensionalization of variables is also performed for computational convenience: the frequencies are divided by the natural frequency of the resonant mode; the vibration amplitudes are divided by the shell thickness h. The resulting $2 \times$ d.o.f.

equations are studied by using (i) the software AUTO 97 [37] for continuation and bifurcation analysis of non-linear ordinary differential equations, and (ii) direct integration of the equations of motion by using the DIVPAG routine of the Fortran library IMSL. Continuation methods allow one to follow the solution path, with the advantage that unstable solutions can also be obtained; these are not ordinarily attainable using direct numerical integration. The software AUTO 97 is capable of extending the solution, bifurcation analysis and branch switching by using arclength continuation and collocation methods. In particular, the shell response under harmonic excitation has been studied by using an analysis in two steps: (i) first the excitation frequency has been fixed far enough from resonance and the magnitude of the excitation has been used as a bifurcation parameter; the solution has been started at zero force where the solution is the trivial undisturbed configuration of the shell and has been continued up to reach the desired force magnitude; (ii) when the desired magnitude of excitation has been reached, the solution has been continued by using the excitation frequency as the bifurcation parameter.

All calculations, with the exception of those in Section 6.1.1, have been performed for a shell having the following dimensions and material properties: $L=520\,\text{mm}$, $R=149.4\,\text{mm}$, $h=0.519\,\text{mm}$, $E=1.98\times10^{11}\,\text{Pa}$, $\rho=7800\,\text{kg/m}^3$ and $v=0.3$. The shell was considered empty in Sections 6.1 and 6.4, completely water-filled with zero pressure on the fluid at the shell ends in Section 6.2 ($\rho_F=1000\,\text{kg/m}^3$) and water-filled with geometric imperfections in Section 6.3. Comparison of present results to those available in the literature for an empty shell is given in Section 6.1.1. In Section 6.3 theoretical results are compared to experimental results for a water-filled shell reported in Ref. [10] for validation purposes. More results are presented for the water-filled shell, see Section 6.2, than for the empty shell as a consequence of the fact that the presence of a liquid largely enhances the softening type non-linearity of the response, as observed theoretically and experimentally [10]. Therefore, a non-linear study is much more important for the water-filled shell than for the empty one. Convergence of the solution with the number of terms in the expansion and effect of removing the additional term $\hat{u}$ are presented only in Section 6.2. Finally in Section 6.4 the effects of static axial loads and radial pressure on the non-linear shell response have been investigated.

6.1. Empty shell

The response of the circular cylindrical shell subjected to harmonic point excitation of 2 N applied in the middle of the shell in the neighbourhood of the lowest (fundamental) resonance $\omega_{1,n}=2\pi\times215.3\,\text{rad/s}$, corresponding to mode ($m=1$, $n=5$), is given in Fig. 2; only the principal (resonant) co-ordinates, corresponding to driven and companion modes, are shown for brevity. The Flügge–Lur'e-Byrne non-linear theory of shells has been used in the calculation, with modal damping $\zeta_{1,n}=0.001(\zeta_{1,n}=\zeta_{1,n,c\text{ or }s})$. All the calculations reported in this section, if not diversely specified, have been performed by using an expansion involving 16 generalized co-ordinates, as given in Eqs. (19) with the additional term $\left[u_{1,2n,c}(t)\cos(2n\theta)+u_{1,2n,s}(t)\sin(2n\theta)\right]\cos(\lambda_1 x)$ in Eq. (19a). The solution initially presents a single branch "1" with a folding and a typical softening-type behaviour and corresponds to a driven mode vibration with zero amplitude of the companion mode. Branch "1" presents a pitchfork bifurcation around the peak of the response where branch "2" arises and where branch "1" loses stability. Branch "2" is the solution with participation of both driven and companion modes, giving a standing wave plus a travelling wave

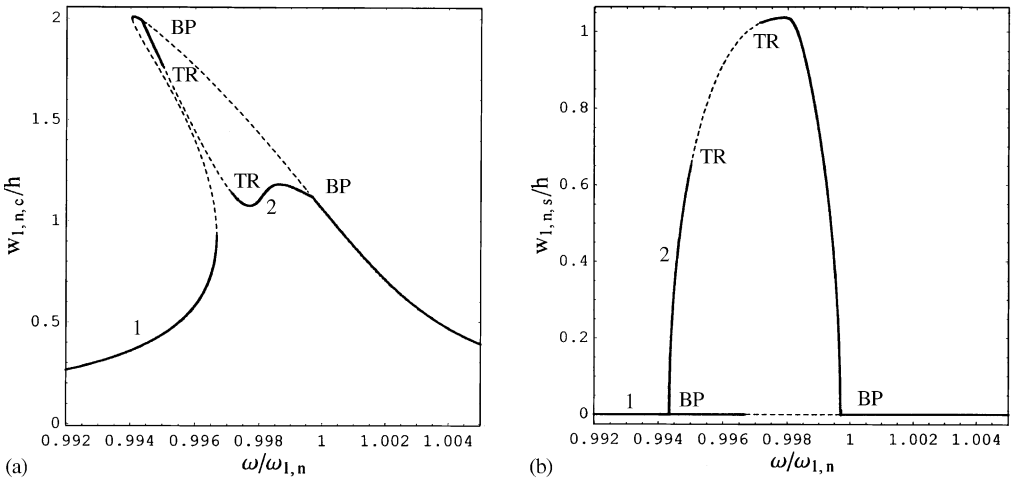

Fig. 2. Response amplitude—frequency relationship for the fundamental mode of the perfect, empty shell using Flügge–Lur'e-Byrne theory ($\varsigma_{1,n} = 0.001$) reporting only resonant generalized co-ordinates: (a) amplitude of $w_{1,n,c}(t)$, driven mode; (b) amplitude of $w_{1,n,s}(t)$, companion mode. 1, branch "1"; 2, branch "2"; BP, pitchfork bifurcation; TR, Neimark-Sacher bifurcation.

response around the shell. Branch "2" loses stability at a Neimark–Sacker (torus) bifurcation where amplitude modulations of the solution arise; modulations end at a second Neimark–Sacker bifurcation. The response between the two Neimark–Sacker bifurcations is quasi-periodic and the Poincaré map shows a limit cycle, as observed by Amabili et al. [9] by using the Donnell's shallow-shell theory. Branch "2" ends at a second pitchfork bifurcation where it merges with branch "1" to regain stability. A qualitatively similar behaviour has been found in previous studies based on different shell theories and different solution methods; see, e.g., Refs. [4,6,8–10,21].

The response of the shell in the time domain is given in Figs. 3 and 4 for excitation frequency $\omega/\omega_{1,n} = 0.998$ (stable response on branch "2") and 0.9969 (unstable response on both branches "1" and "2"), respectively. In Figs. 3(a–c) the generalized co-ordinates associated with driven, companion and first axisymmetric modes are reported. It is clearly shown that the phase difference between driven and companion modes is $\theta_2 - \theta_1 \cong \pi/2$, giving a travelling wave response. The relative amplitudes among the generalized co-ordinates $u_{1,n,c/s}$, $v_{1,n,c/s}$ and $w_{1,n,c/s}$ associated with driven and companion modes are almost the same of the one observed for linear free vibrations (eigenvectors of the linear solution). Only very small variations of the relative amplitudes are observed for these modes in the neighbourhood of the resonance. However, this is not true for all the other generalized co-ordinates. When the excitation has a frequency close to the resonance of mode ($m = 1$, n), results show that the generalized co-ordinates associated with driven and companion modes ($m = 1$, n) have the same frequency of the excitation. The co-ordinates associated with modes ($m = 1$, $2n$) and ($m = 3$, $2n$) and all the co-ordinates associated to axisymmetric modes, as shown in Fig. 3(c), have twice the frequency of the excitation; the co-ordinates associated with modes ($m = 3$, n), ($m = 1$, $3n$) and ($m = 3$, $3n$) have three times the frequency of the excitation. Fig. 3(c) also shows a negative (inward) axisymmetric oscillation of the shell associated with large-amplitude asymmetric vibration; this is a characteristic of non-linear vibrations of circular cylindrical shells. Figs. 4(a), (b) show that the response has

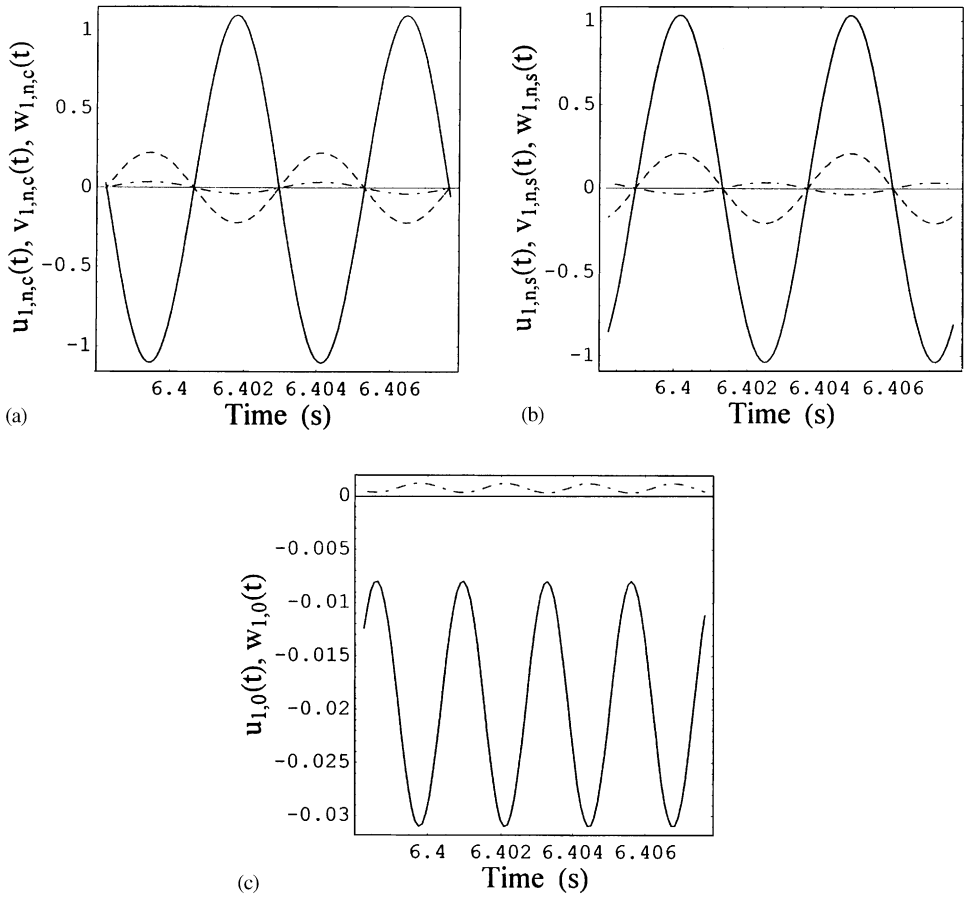

Fig. 3. Time response of the shell for a travelling wave using Flügge–Lur'e-Byrne theory ($\omega/\omega_{1,n} = 0.998$). (a) Generalized co-ordinates associated with the driven mode; ——, $w_{1,n,c}(t)$; – –, $v_{1,n,c}(t)$; – · –, $u_{1,n,c}(t)$. (b) Generalized co-ordinates associated with the companion mode; ——, $w_{1,n,s}(t)$; – –, $v_{1,n,s}(t)$; – · –, $u_{1,n,s}(t)$. (c) Generalized co-ordinates associated with the first axisymmetric mode; ——, $w_{1,0}(t)$; – · –, $u_{1,0}(t)$.

amplitude-modulations (quasi-periodic) between the two Neimark–Sacher bifurcations, where no stable solution are indicated in Fig. 2.

Now that the non-linear response of the shell in the spectral neighbourhood of the fundamental resonance has been understood, it is interesting to compare results obtained by using the same approach and different shell theories. In Fig. 5 branch "1" of the solution has been computed with the present Lagrangian approach by using (i) Donnell's, (ii) Sanders–Koiter, (iii) Flügge–Lur'e-Byrne and (iv) Novozhilov's non-linear shell theories. Results obtained by using Donnell's non-linear shallow-shell theory, computed by using the mode expansion given by Eq. (19c) and the approach reported in Refs. [7–10], are also given for comparison. For this case, results from Novozhilov's non-linear theory of shell are practically coincident with those of Flügge–Lur'e-Byrne theory and therefore are not reported in Fig. 5. Moreover, differences between Flügge–Lur'e-Byrne and Sanders–Koiter theories are absolutely negligible. For practical applications the

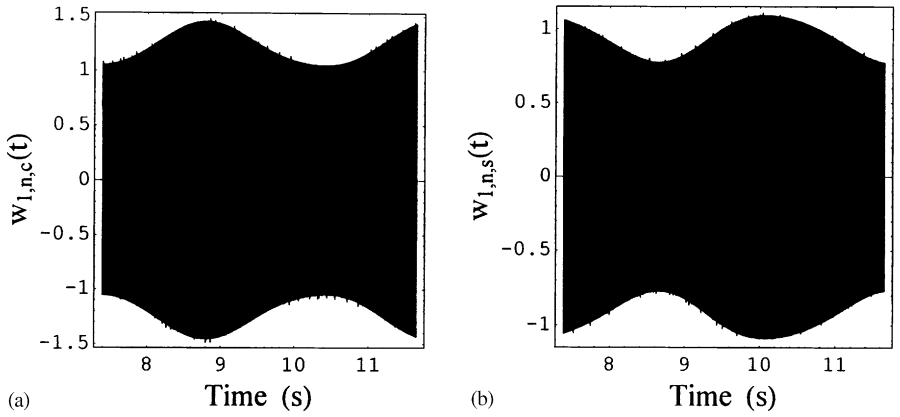

Fig. 4. Time response of the shell in case of amplitude modulations (limit cycle) using Flügge–Lur'e-Byrne theory ($\omega/\omega_{1,n} = 0.9969$); (a) Generalized co-ordinate $w_{1,n,c}(t)$ associated with the driven mode. (b) Generalized co-ordinate $w_{1,n,s}(t)$ associated with the companion mode.

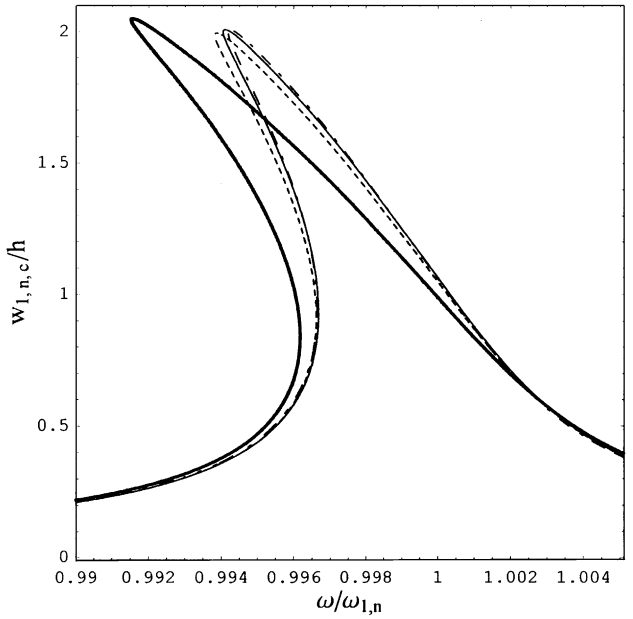

Fig. 5. Response amplitude—frequency relationship for the fundamental mode of the perfect, empty shell; branch "1" only ($\varsigma_{1,n} = 0.001$) reporting only the generalized co-ordinate $w_{1,n,c}(t)$. ▬, Donnell's non-linear shallow-shell theory; – –, Donnell's theory (Lagrangian approach); – · –, Sanders–Koiter theory; ——, Flügge–Lur'e-Byrne theory (coincident with Novozhilov).

difference between Flügge–Lur'e-Byrne and Donnell's (present Lagrangian approach) theories can be considered very small as well. However, although all the results obtained by using the present Lagrangian approach are very close to each other, differences with Donnell's non-linear shallow-shell theory are quite significant; in particular, an excessive softening non-linearity is

predicted by Donnell's non-linear shallow-shell theory. In fact, this theory neglects in-plane inertia, which plays a relevant role in axisymmetric modes. In this case, Donnell's non-linear shallow-shell theory gives a wrong evaluation of the linear natural frequency of the first axisymmetric mode, and it explains the difference with all the other theories. It is interesting to observe that the mode investigated has $n=5$ circumferential waves, which is a number almost at the limit of applicability of the Donnell's shallow-shell theory.

6.1.1. Comparison with results available in literature

In this subsection only, numerical results for a different shell are carried out in order to compare present results to those available in the literature. Calculations have been performed for a simply supported, empty shell previously studied by Chen and Babcock [4], Pellicano et al. [34], Varadan et al. [38] and Ganapathi and Varadan [39]. Dimensions and material properties are: $L=0.2\,\mathrm{m}$, $R=0.1\,\mathrm{m}$, $h=0.247\,\mathrm{mm}$, $E=71.02\times10^9\,\mathrm{Pa}$, $\rho=2796\,\mathrm{kg/m^3}$ and $\nu=0.31$. A harmonic force excitation $\tilde{f}=0.0785\,N$ and modal damping $\zeta_{1,n}=0.0005$ are assumed. Donnell's theory, retaining in-plane inertia, has been used with 36 d.o.f. In particular, the 36 generalized co-ordinates used are given by Eqs. (18a)–(18c) by inserting $j=k\times n$, $n=5$ for the fundamental mode, $k=1,\ldots,4$; $M_1=3$ if $k=2$, $M_1=1$ otherwise (odd m only); $M_2=5$ (odd m only). Only the fundamental mode ($n=6$, $m=1$) is investigated; it has a natural frequency of 555.9 Hz. The shell response is shown in Fig. 6 and is compared to the response calculated by Pellicano et al. [34], who used Donnell's non-linear shallow-shell theory with a mode expansion involving 23 d.o.f., to the

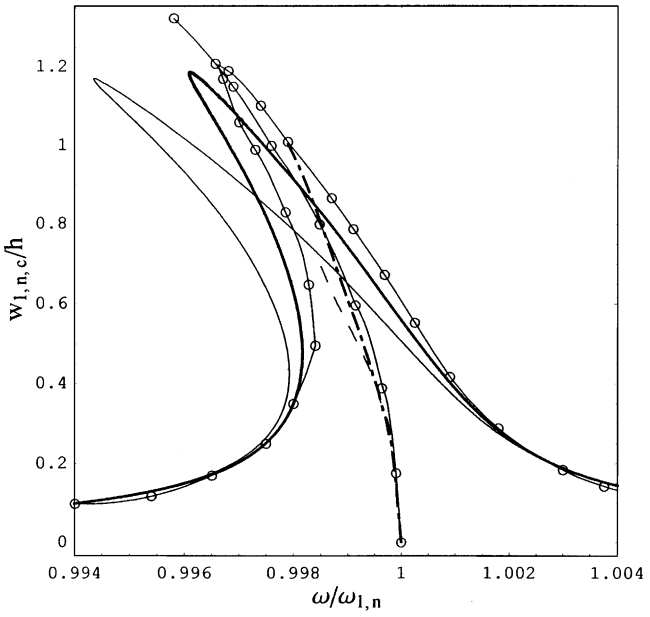

Fig. 6. Response amplitude—frequency relationship for the fundamental mode of the perfect, empty shell studied by Chen and Babcock [4] (branch "1" only) with only the generalized co-ordinate, $w_{1,n,c}(t)$, reported. ——, present study (Donnell's theory, Lagrangian approach); ——, backbone curve and shell response from Ref. [34] (Donnell's non-linear shallow-shell theory); —○—, backbone curve from Ref. [4]; – · –, results from Ref. [38]; —·—, backbone curve from Ref. [39].

response calculated by Chen and Babcock [4], who used the perturbation method to solve the non-linear equations obtained by Donnell's non-linear shallow-shell theory, and to the backbone curves (indicating only the resonance, i.e., the peak of the response) computed by Varadan et al. [38], who used a simple three-mode expansion and Donnell's non-linear shallow-shell theory, and by Ganapathi and Varadan [39], who used the finite element method based on Novozhilov's shell theory. Present results are intermediate between those obtained by Pellicano et al. [34] and those obtained by Ganapathi and Varadan [39] and are close to those of Chen and Babcock [4]. This can be considered a good validation of the present model.

6.2. *Water-filled shell*

The response of the water-filled, circular cylindrical shell subjected to harmonic point excitation of 3 N applied in the middle of the shell in the neighbourhood of the lowest (fundamental) resonance $\omega_{1,n} = 2\pi \times 76.15$ rad/s, corresponding to mode ($m = 1$, $n = 5$), is given in Fig. 7; only the principal (resonant) co-ordinates, corresponding to driven and companion modes, are shown for brevity. The Sanders–Koiter non-linear theory of shells has been used in the calculation, with modal damping $\zeta_{1,n} = 0.0017$. All the calculations reported in this section, if not diversely specified, have been performed by using an expansion involving the 16 generalized co-ordinates specified in Section 6.1. The response is qualitatively close to the one of the fundamental mode of the empty shell (see Fig. 2); the main difference is the peak on branch "2" close to the second pitchfork bifurcation in Fig. 7. From the quantitative point of view the change is much more important because the frequency scale is largely enlarged; it means that the water-filled shell presents a largely enhanced non-linear behaviour of softening type with respect to the same empty shell. The comparison among the different non-linear shell theories is given in Fig. 8, where both branches "1" and "2" are reported for the "predominant" generalized co-ordinate $w_{1,n,c}(t)$. In

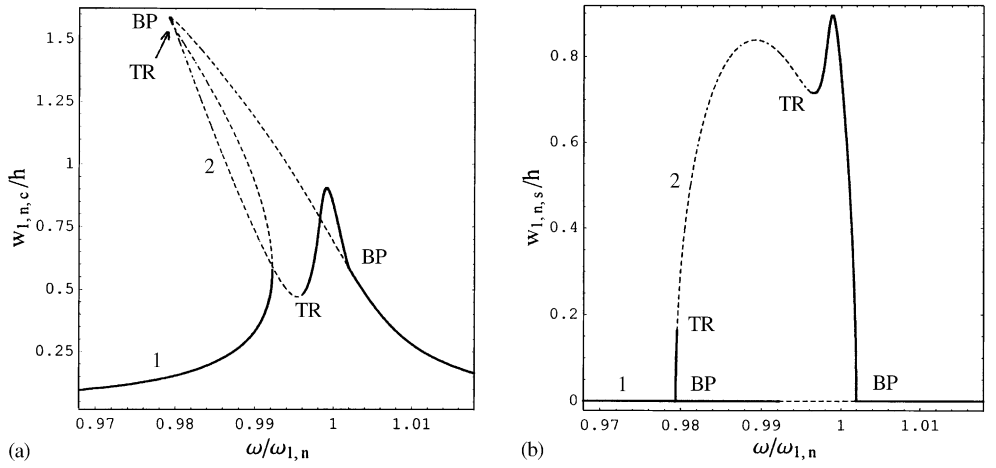

Fig. 7. Response amplitude—frequency relationship for the fundamental mode of the perfect, water-filled shell ($\varsigma_{1,n} = 0.0017$; $\tilde{f} = 3$N); using Sanders–Koiter theory, and only reporting the resonant generalized co-ordinates. (a) Amplitude of $w_{1,n,c}(t)$, driven mode; (b) amplitude of $w_{1,n,s}(t)$, companion mode. 1, branch "1"; 2, branch "2"; BP, pitchfork bifurcation; TR, Neimark–Sacher bifurcation.

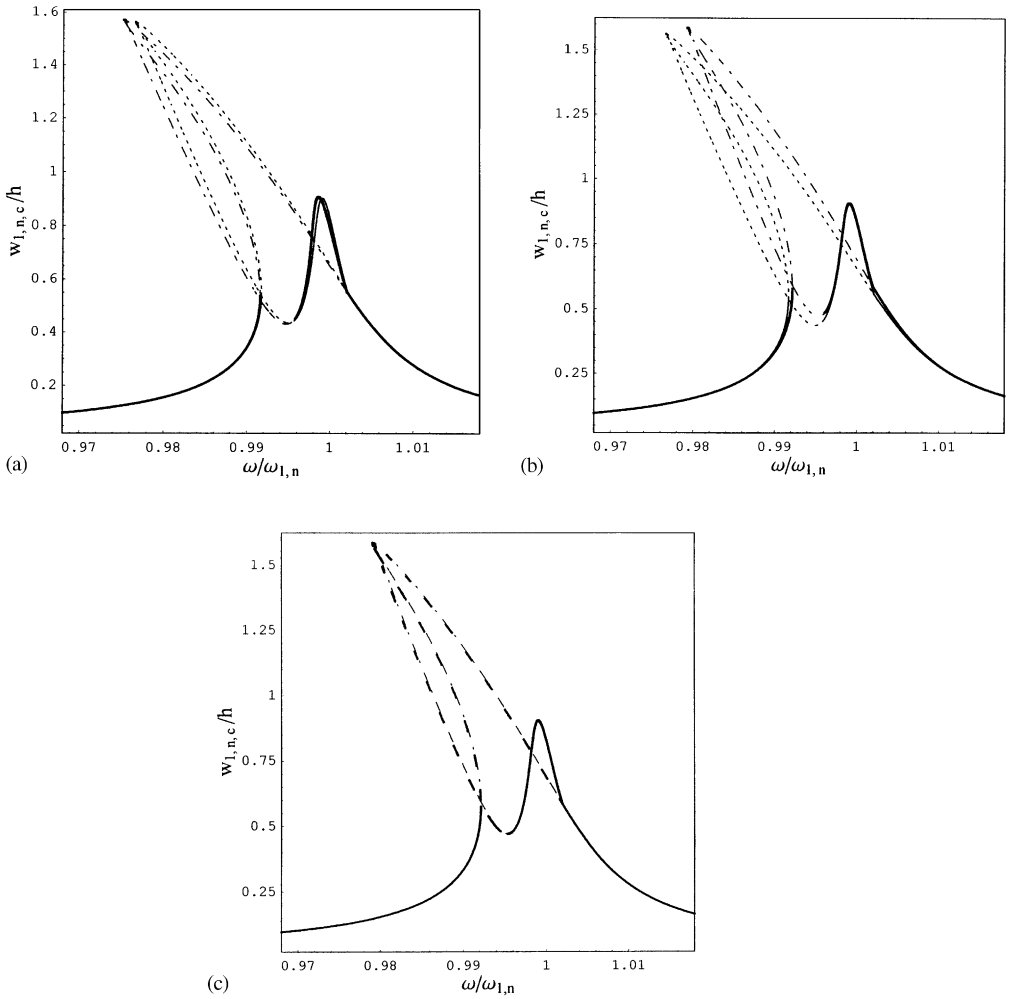

Fig. 8. Response amplitude—frequency relationship for the fundamental mode of the perfect, water-filled shell for branch "1" ($\varsigma_{1,n} = 0.0017$; $\tilde{f} = 3$ N), only reporting $w_{1,n,c}(t)$. (a) $-\cdot-$, Donnell's non-linear shallow-shell theory; $--$, Donnell's theory (Lagrangian approach). (b) $--$, Donnell's non-linear shallow-shell theory; $-\cdot-$, Sanders–Koiter theory. (c) $-\cdot-$, Sanders–Koiter theory; $--$ Flügge–Lur'e-Byrne theory (coincident with Novozhilov).

particular, results for the Lagrangian approach by using the (i) Donnell's, (ii) Sanders–Koiter (iii) Flügge–Lur'e-Byrne and (iv) Novozhilov's non-linear shell theories and results obtained by using Donnell's non-linear shallow-shell theory are compared. Novozhilov's, Flügge–Lur'e-Byrne and Sanders–Koiter theories give practically coincident results (as previously, results for the Novozhilov's theory are not reported in Fig. 8; Flügge–Lur'e-Byrne and Sanders–Koiter theories are compared in Fig. 8(c) but the curves are practically superimposed). Fig. 8(a) shows that the difference between Donnell's non-linear shallow-shell theory and Donnell's theory with the present Lagrangian approach (retaining in-plane inertia) is much smaller for the water-filled shell than for the empty case. A significant, but not large, difference between Sanders–Koiter (therefore also Flügge–Lur'e-Byrne and Novozhilov's) and Donnell's theories is shown in Fig. 8(b).

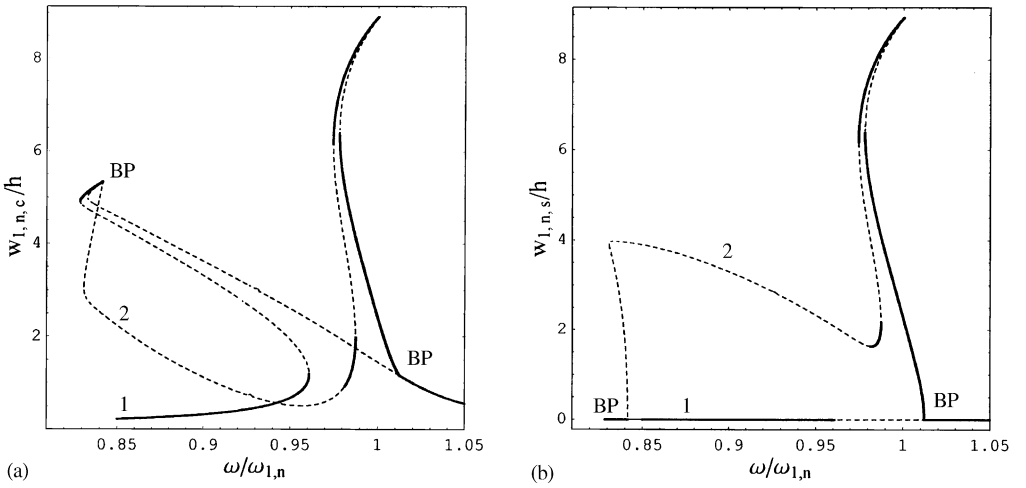

Fig. 9. Response amplitude—frequency relationship for the fundamental mode of the perfect, water-filled shell ($\varsigma_{1,n} = 0.0017$; $\tilde{f} = 30$ N); using Donnell's theory (Lagrangian approach). (a) Amplitude of $w_{1,n,c}(t)$, driven mode; (b) amplitude of $w_{1,n,s}(t)$, companion mode. 1, branch "1"; 2, branch "2"; BP, pitchfork bifurcation.

In order to investigate if the difference among the shell theories becomes larger by increasing the vibration amplitude, the same shell subjected to excitation of 30 N has been investigated. Fig. 9 presents the response computed by using the present Lagrangian approach and the Donnell's non-linear shallow-shell theory. Large qualitative differences between Figs. 7 and 9 are evident. In particular, the peak on branch "2" close to the second bifurcation is largely increased with respect to the other part of the response and the frequency range without simple periodic responses is enlarged. The comparison among the different shell theories is given in Fig. 10; in this case as well differences among Donnell's non-linear shallow-shell, Donnell's with Lagrangian approach and Sanders–Koiter theories are significant, but not excessive.

It can be concluded from these results that Donnell's non-linear shallow-shell theory is much more accurate for water-filled than for empty shells. This can be easily explained by the fact that the in-plane inertia, which is neglected by Donnell's non-linear shallow-shell theory, is much less important for a water-filled shell that has a large radial inertia due to the liquid associated to radial deflection.

The effect of neglecting the additional term $\hat{u}$, see Eqs. (24)–(34), is investigated in Fig. 11 for Donnell's theory with Lagrangian approach. The difference is small and the additional term $\hat{u}$ can be neglected without a significant difference in the computed response. Similar effect of $\hat{u}$ has been found for the other shell theories.

A crucial point of the present Lagrangian approach is the expansion of the middle surface displacements. The expansion given by Eqs. (19a)–(19c) has been compared with reduced and enlarged expansions in Fig. 12 for Donnell's theory with Lagrangian approach. In particular, results show that the expansion given by Eqs. (19a)–(19c) is the smallest one necessary to obtain correct results. The expansion with 16 d.o.f. used in all the previous calculations gives results very close to this one. A largely increased expansion with 36 d.o.f., which can be considered close to convergence, gives a shell response relatively close to the one computed with 14 d.o.f. In

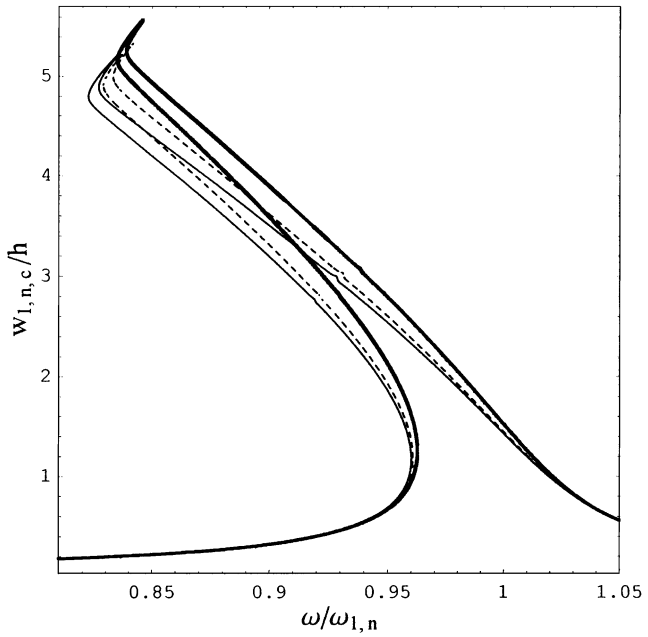

Fig. 10. Response amplitude—frequency relationship for the fundamental mode of the perfect, water-filled shell for branch "1" ($\varsigma_{1,n} = 0.0017$; $\tilde{f} = 30$ N), reporting only $w_{1,n,c}(t)$. ——, Donnell's non-linear shallow-shell theory; – –, Donnell's theory (Lagrangian approach); ▬, Sanders–Koiter theory.

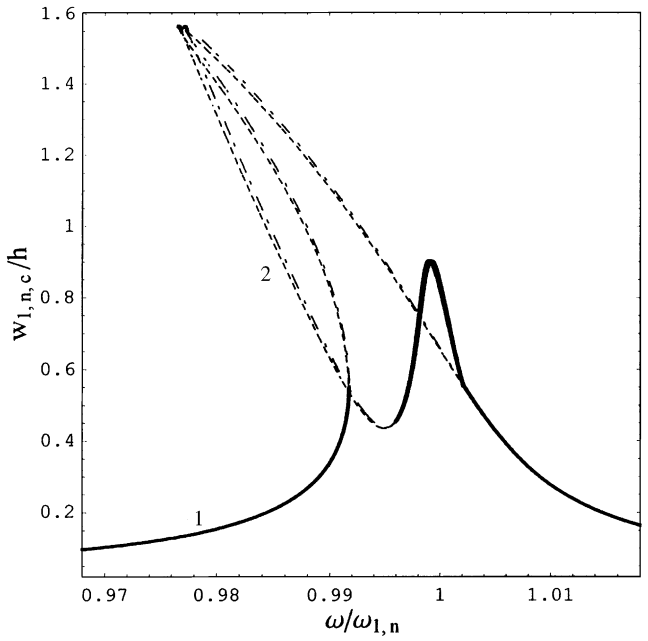

Fig. 11. Response amplitude—frequency relationship for the fundamental mode of the perfect, water-filled shell ($\varsigma_{1,n} = 0.0017$; $\tilde{f} = 3$ N) using Donnell's theory (Lagrangian approach): –·–, solution with $\hat{u}$; – –, solution neglecting $\hat{u}$. 1, branch "1"; 2, branch "2".

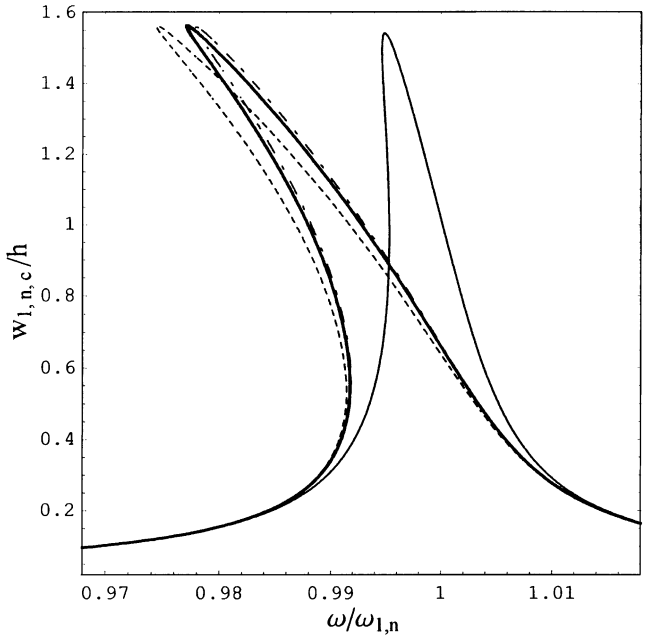

Fig. 12. Convergence of the response amplitude—frequency relationship for the fundamental mode of the perfect, water-filled shell of branch "1" only ($\varsigma_{1,n} = 0.0017$; $\tilde{f} = 3$ N); using Donnell's theory (Lagrangian approach): ——, 12 d.o.f. model; –·– 14 d.o.f. model, Eq. (19a)–(c); ▬, 16 d.o.f. model; ––, 36 d.o.f. model.

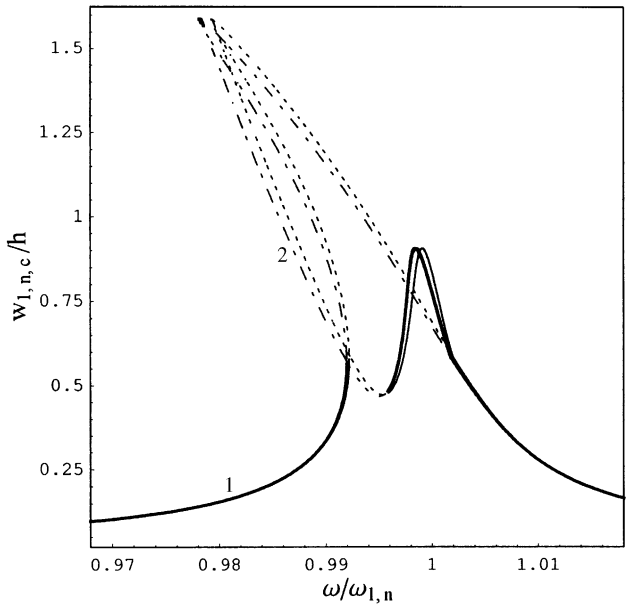

Fig. 13. Convergence of the response amplitude—frequency relationship for the fundamental mode of the perfect, water-filled shell ($\varsigma_{1,n} = 0.0017$; $\tilde{f} = 3$ N) using Sanders–Koiter theory: ––, 16 d.o.f. model; –·–, 26 d.o.f. model. 1, branch "1"; 2, branch "2".

particular, the 36 generalized co-ordinates used in the largest model are given by Eqs. (18a)–(18c) by inserting $j = k \times n$, $n = 5$ for the fundamental mode, $k = 1, \ldots, 4$; $M_1 = 3$ if $k = 2$, $M_1 = 1$ otherwise (odd m only); $M_2 = 5$ (odd m only). On the other hand, as shown by the 12 d.o.f. model, if the generalized co-ordinates $v_{3,2n,c}$ and $v_{3,2n,s}$ are removed from Eqs. (19a)–(19c), a completely wrong response is obtained.

The convergence of the solution for other shell theories is very similar. In particular, Fig. 13 shows the shell response computed by using the Sanders–Koiter shell theory and expansions with 16 and 26 d.o.f. The 26 generalized co-ordinates are given by Eqs. (18a)–(18c) by inserting $j = k \times n$, $n = 5$, $k = 1, \ldots, 3$, $M_1 = 1$ and $M_2 = 5$ with odd m only.

6.3. Water-filled shell with imperfections

The effect of geometric imperfections on the natural frequency of the fundamental mode of the water-filled shell is investigated in Figs. 14(a)–(14c) for both the Donnell's (Lagrangian approach) and Sanders–Koiter theories with expansion involving 48 d.o.f. Natural frequencies are evaluated by eliminating all the non-linear terms in the generalized co-ordinates (but not non-linear terms associated with imperfections) from the Lagrange equations. The 48 generalized co-ordinates are given by Eqs. (18a)–(18c) inserting $j = k \times n$, $n = 5$, $k = 1, \ldots, 4$; $M_1 = 1$ if $k = 4$, $M_1 = 3$ otherwise (odd m only); $M_2 = 5$ (odd m only). In particular, three different geometric imperfections are considered: (i) axisymmetric imperfection $\tilde{A}_{1,0}$, (ii) asymmetric imperfection $\tilde{A}_{1,n}$ having the same shape of the fundamental mode, and (iii) asymmetric imperfection $\tilde{A}_{1,2n}$ having twice the number

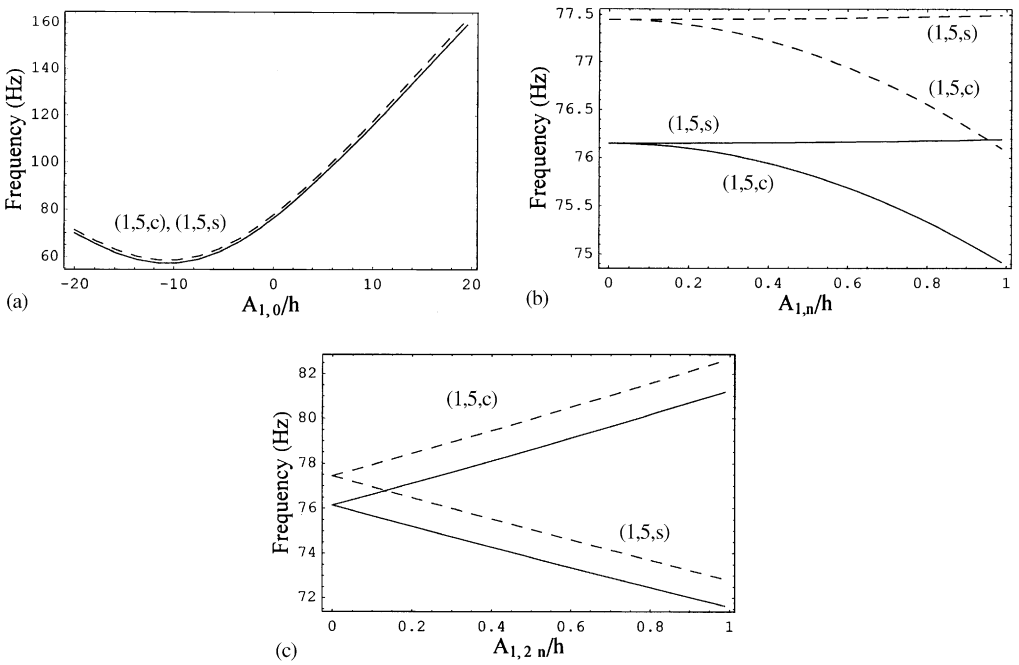

Fig. 14. Natural frequency of the fundamental mode ($n = 5$, $m = 1$) of the water-filled shell versus the amplitude of geometric imperfections. (a) Axisymmetric imperfection $\tilde{A}_{1,0}$; (b) asymmetric imperfection $\tilde{A}_{1,n}$; (c) asymmetric imperfection $\tilde{A}_{1,2n}$. – –, Donnell's theory (Lagrangian approach); ——, Sanders–Koiter theory.

of circumferential waves of the fundamental mode. The axisymmetric imperfection does not divide the double eigenvalue associated with the fundamental mode; this is only obtained by asymmetric imperfections. Positive axisymmetric imperfections (outward Gaussian curvature) increase the natural frequency; small negative axisymmetric imperfections (inward gaussian curvature) decrease it, but the trend is inverted around $\tilde{A}_{1,0} \cong -10h$. Imperfections having twice the number of circumferential waves with respect to the resonant mode have a very large effect on its natural frequency, as indicated in Fig. 14(c) (note that curves cross at zero imperfection in this case and that the position of modes (1, 5, *c*) and (1, 5, *s*) is inverted for negative imperfections); imperfections with the same number of circumferential waves of the fundamental mode have a smaller effect, but still quite large. Imperfections with a number of circumferential waves that is not a multiple of n play a very small role as it has been shown in Ref. [10]. The main difference between Donnell's and Sanders–Koiter results is related to the calculation of the natural frequency of the fundamental mode for zero imperfection; the effect of imperfections on the frequency is almost the same for both the theories.

The response of a simply supported, water-filled stainless-steel shell experimentally tested by Amabili [10] is computed by using Donnell's non-linear shell theory (Lagrangian approach) with the 36 d.o.f. model specified in the previous section. Results are compared to the experimental results reported in Ref. [10] for validation purposes. The fundamental mode ($m=1$, $n=5$) is investigated. The modal damping used in the calculation is $\zeta_{1,n} = 0.0017$ and the excitation is given by a harmonic radial force of 3 N applied at $x=L/2$ and $\theta=0$. A geometric imperfection $A_{1,2n} = -0.147\,h$ has been used to reproduce the difference between the natural frequency of driven and companion modes. These two natural frequencies are theoretically equal (they are associated with the same mode, shifted angularly by $\pi/(2n)$) for the symmetry of the shell. However, due to small imperfections in the test specimens (small imperfections are always present in actual structures), these two natural frequencies present a small difference. Due to the geometric imperfections, driven ($w_{1,5,c}(t)$) and companion ($w_{1,5,s}(t)$) modes are both directly excited by the external force (therefore the denomination driven and companion modes loses its meaning). Two sensors were used in the experiments to measure shell vibrations. The circumferential distance $R\theta$ of the two vibration sensors from the excitation point was: 26.5 and –21 mm for the first and second sensors, respectively. The sensors were placed at nodes of modes $w_{1,5,c}(t)$ and $w_{1,5,s}(t)$; therefore each sensor measures a single co-ordinate. The comparison is shown in Fig. 15, where a good agreement between theoretical and experimental results is shown. In particular, the agreement is excellent for the second peak.

6.4. *Effect of constant axial load and pressure on the non-linear response of the empty shell*

The effects of a uniform and constant axial load per unit length N on the response to harmonic excitation of the fundamental mode ($m=1$, $n=5$) of the empty shell have been investigated. The Sanders–Koiter non-linear theory has been used. The mode expansion involves 22 d.o.f.; they are those used in the previous model with 16 d.o.f. but with $M_2=9$ (odd m only). This addition of axisymmetric modes is necessary in case of pressurization or axial loads in order to predict with accuracy the static deformation and pre-stress of the shell. The stability of the shell under static axial compressive load N is shown in Fig. 16, where the post-buckling behaviour of the shell (without companion mode participation) corresponds to branch "2", which starts at a pitchfork

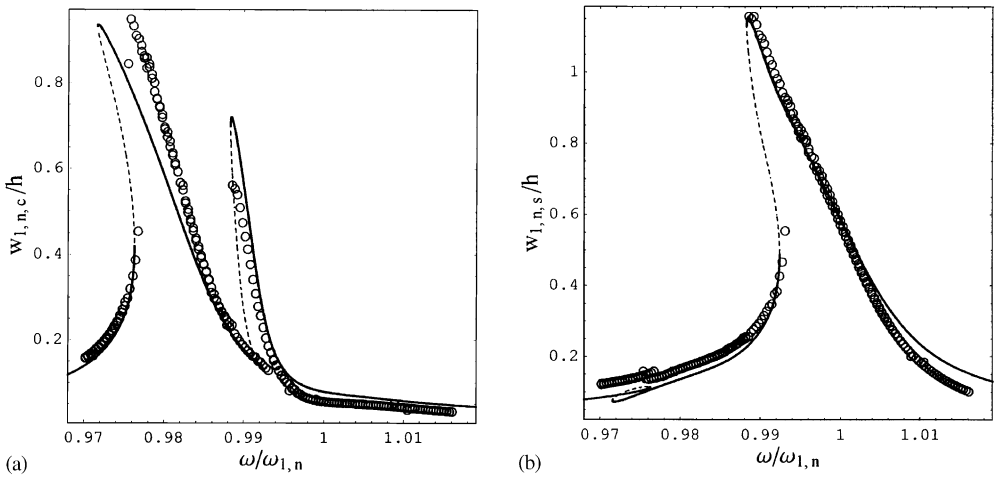

Fig. 15. Response amplitude—frequency relationship for the fundamental mode of the water-filled imperfect shell ($\varsigma_{1,n} = 0.0017$; $\tilde{f} = 3$ N): ◦◦◦, experimental data; ——, stable theoretical solutions; – – –, unstable theoretical solutions. (a) Vibration amplitude/h from the first sensor; (b) vibration amplitude/h from the second sensor.

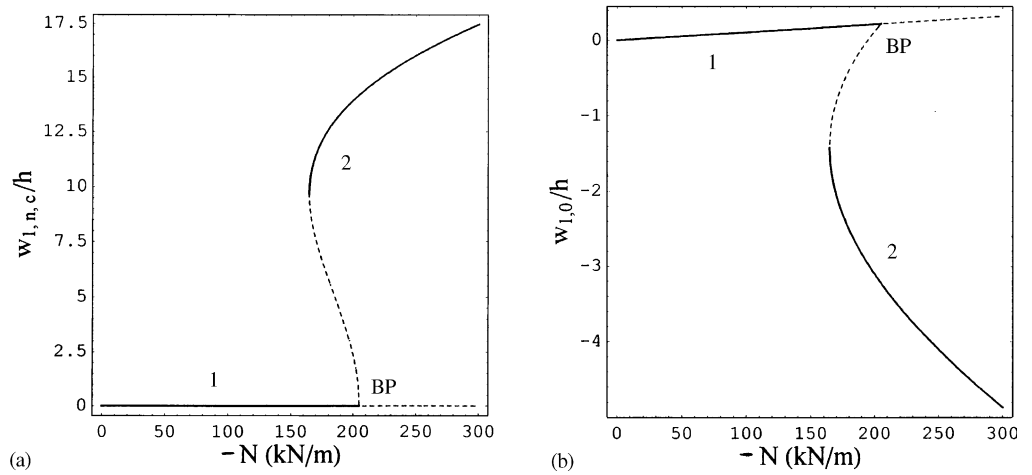

Fig. 16. Buckling and post-buckling of the empty shell under static axial load per unit length N: (a) generalized co-ordinate $w_{1,n,c}$; (b) generalized co-ordinate $w_{1,0}$. 1, branch "1"; 2, branch "2"; BP, pitchfork bifurcation.

bifurcation point, indicating buckling, at $N = -205$ kN/m. The bifurcation of the equilibrium is slightly subcritical; this behaviour is characteristic of softening-type systems. The mode that goes first in instability is the fundamental mode of vibration ($m = 1$, $n = 5$) in this case. The simple formula $N_{cr} = Eh^2/(R\sqrt{3(1-\nu^2)})$ [28] gives a buckling load per unit length $N_{cr} = 216 \times 10^3$ N/m, which is very close to the bifurcation point found in Fig. 16. The non-linear response of the shell under harmonic force of 2 N, damping $\zeta_{1,n} = 0.001$ and axial load $N = -150$ kN/m is shown in Fig. 17. The axial load decreases the natural frequency of the shell to about $0.51\omega_{1,n}$. By

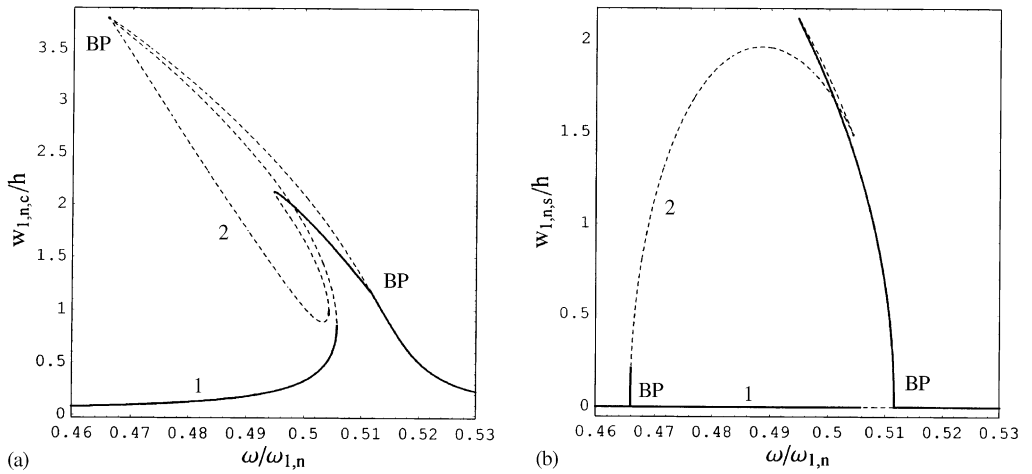

Fig. 17. Response amplitude—frequency relationship for the fundamental mode of the perfect, empty shell under axial load ($N=-150\,kN/m$; $\varsigma_{1,n}=0.001$); using Sanders–Koiter theory: (a) amplitude of $w_{1,n,c}(t)$, driven mode; (b) amplitude of $w_{1,n,s}(t)$, companion mode. 1, branch "1"; 2, branch "2"; BP, pitchfork bifurcation.

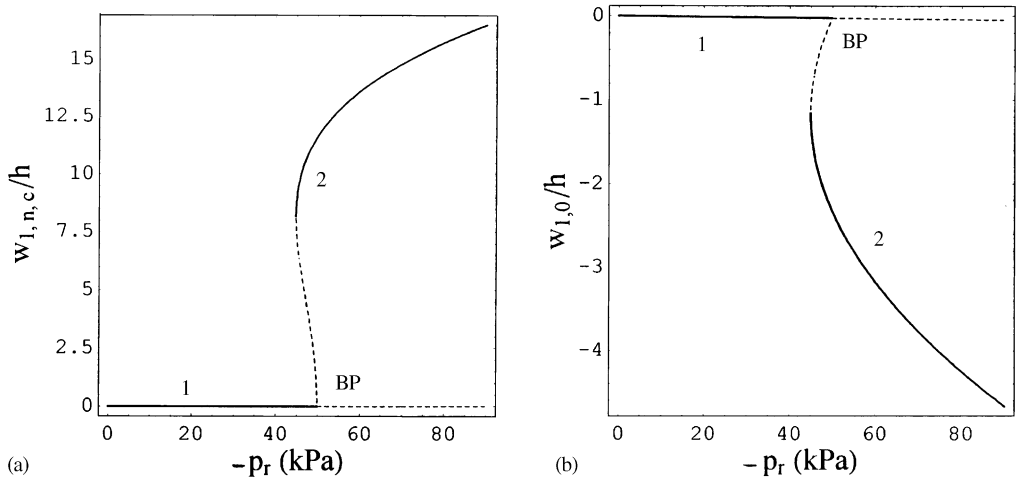

Fig. 18. Buckling and post-buckling of the empty shell under pressure p_r: (a) generalized coordinate $w_{1,n,c}$; (b) generalize co-ordinate $w_{1,0}$. 1, branch "1"; 2, branch "2"; BP, pitchfork bifurcation.

comparing Figs. 17 and 2, which has been obtained for the same case without static load, it is evident that a compressive axial load largely increases the softening-type non-linearity of the shell.

The effect of external uniform pressure has been investigated with the same model. The stability of the shell under pressure p_r is shown in Fig. 18 for mode ($m=1$, $n=5$). Buckling is reached for $p_r=-49.9\,kPa$ (external pressure). Comparison of Figs. 16(b) and 18(b) shows that a larger pre-buckling deformation (specifically, in opposite direction) is obtained under axial load than under pressure. The mode that goes first in instability is the mode ($m=1$, $n=6$) for p_r about $-38\,kPa$ in this case; the fundamental mode of vibration ($m=1$, $n=5$) reaches instability just after this one. The non-linear response of the shell under harmonic force of 2 N, damping $\zeta_{1,n}=0.001$ and

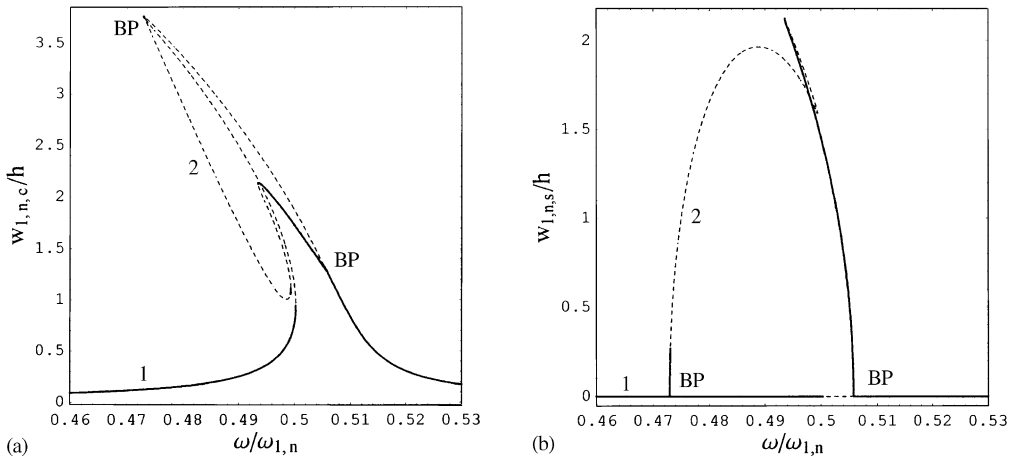

Fig. 19. Response amplitude—frequency relationship for the fundamental mode of the perfect, empty shell under pressure ($p_r = -37$ kPa; $\varsigma_{1,n} = 0.001$); uisng Sanders–Koiter theory: (a) amplitude of $w_{1,n,c}(t)$, driven mode; (b) amplitude of $w_{1,n,s}(t)$, companion mode. 1, branch "1"; 2, branch "2"; BP, pitchfork bifurcation.

pressure $p_r = -37$ kPa is shown in Fig. 19. The imposed external pressure decreases the natural frequency of the shell to about $0.51\omega_{1,n}$, as in the previous case. By comparing Figs. 19 and 20 it is evident that an external pressure largely increases the softening type non-linearity of the shell, as observed in Fig. 17 for compressive axial load.

Geometric imperfections are not considered in this section. As it is very well known, geometric imperfections have a large effect on the buckling of axially compressed shells.

7. Conclusions

The response of an empty and simply supported circular cylindrical shell has been computed by using five classical non-linear shell theories: (i) Donnell's shallow-shell, (ii) Donnell's with in-plane inertia, (iii) Sanders–Koiter, (iv) Flügge–Lur'e-Byrne and (v) Novozhilov's theories. Results for theory (i) has been obtained by using the approach developed in Refs. [7–10]; for all the other theories, the Lagrangian approach developed in the present study has been used. Results from the Sanders–Koiter, Flügge–Lur'e-Byrne and Novozhilov's theories are extremely close, for both empty and water-filled shells. For the thin shell numerically investigated in this study, for which $h/R \cong 288$, there is almost no difference among them. Appreciable difference, but not particularly large, has been observed between the previous three theories and Donnell's theory with in-plane inertia. On the other hand, Donnell's non-linear shallow-shell theory is the least accurate among the five theories here compared. It predicts excessive softening-type non-linearity for empty shells. However, for water-filled shells, it predicts sufficiently precise results, also for quite large vibration amplitude. The different accuracy of Donnell's non-linear shallow-shell theory for empty and water-filled shell can easily be explained by the fact that the in-plane inertia, which is neglected in Donnell's non-linear shallow-shell theory, is much less important for a water-filled shell, which has a large radial inertia due to the liquid, than for an empty shell.

Contained liquid, compressive axial loads and external pressure increase the softening-type non-linearity of the shell.

The Lagrangian approach developed has the advantage of being suitable for application to different non-linear shell theories, of satisfying exactly the boundary conditions and of being very flexible to structural modifications without complication of the solution procedure.

A minimum mode expansion necessary to capture the non-linear response of the shell in the neighbourhood of a resonance has been determined and convergence of the solution has been numerically investigated.

Acknowledgements

This work was partially supported by the COFIN 2000 grant of the Italian Ministry for University and Research (MURST).

Appendix. Strain energy for orthotropic and symmetric cross-ply laminated composite shells

By applying Love's first approximation assumptions, the stresses σ_x, σ_θ and $\tau_{x\theta}$ are related to the strain for orthotropic homogeneous material by [40]

$$\sigma_x = \frac{E_x}{1-\nu_{x\theta}\nu_{\theta x}}(\varepsilon_x + \nu_{\theta x}\varepsilon_\theta), \quad \sigma_\theta = \frac{E_\theta}{1-\nu_{x\theta}\nu_{\theta x}}(\varepsilon_\theta + \nu_{x\theta}\varepsilon_x), \quad \tau_{x\theta} = G_{x\theta}\gamma_{x\theta}, \tag{A.1a–c}$$

where E_x and E_θ are Young's moduli in the x and θ directions, respectively, $\nu_{x\theta}$ and $\nu_{x\theta}$ are the Poisson ratios and $G_{x\theta}$ is the shear modulus. The following relationship exists between the Poisson ratios and Young's moduli [40]

$$\nu_{\theta x}E_x = \nu_{x\theta}E_\theta. \tag{A.2}$$

By using Eqs. (10), (A.1) and (A.2), the following expression for the strain energy of orthotropic shells is obtained

$$\begin{aligned} U_S = {} & \frac{1}{2}\frac{E_x h}{1-\nu_{\theta x}^2 E_x/E_\theta}\int_0^{2\pi}\int_0^L \left[\varepsilon_{x,0}^2 + \frac{E_\theta}{E_x}\varepsilon_{\theta,0}^2 + 2\nu_{\theta x}\varepsilon_{x,0}\varepsilon_{\theta,0} + \frac{G_{x\theta}}{E_x}(1-\nu_{\theta x}^2 E_x/E_\theta)\gamma_{x\theta,0}\right] \mathrm{d}x R\,\mathrm{d}\theta \\ & + \frac{1}{2}\frac{E_x h^3}{12(1-\nu_{\theta x}^2 E_x/E_\theta)}\int_0^{2\pi}\int_0^L \left[k_x^2 + \frac{E_\theta}{E_x}k_\theta^2 + 2\nu_{\theta x}k_x k_\theta + \frac{G_{x\theta}}{E_x}(1-\nu_{\theta x}^2 E_x/E_\theta)k_{x\theta}\right] \mathrm{d}x R\,\mathrm{d}\theta \\ & + \frac{1}{2}\frac{E_x\, h^3}{6R(1-\nu_{\theta x}^2 E_x/E_\theta)}\int_0^{2\pi}\int_0^L \Bigg[\varepsilon_{x,0}\, k_x + \frac{E_\theta}{E_x}\varepsilon_{\theta,0}\, k_\theta + \nu_{\theta x}\, \varepsilon_{x,0}\, k_\theta + \nu_{\theta x}\, \varepsilon_{\theta,0}\, k_x \\ & + \frac{G_{x\theta}}{E_x}(1-\nu_{\theta x}^2\, E_x/E_\theta)\varepsilon_{x\theta,0}k_{x\theta}\Bigg] \mathrm{d}x R\,\mathrm{d}\theta. \end{aligned} \tag{A.3}$$

Now the attention is focused on symmetric, laminated composite shells. A laminate is called symmetric when for each layer on one side of the middle surface there is a corresponding identical layer on the other side. It is assumed that each lamina is orthotropic and that each lamina's orthotropic principal directions coincide with the shell co-ordinates; this kind of laminate is referred to as symmetric cross-ply laminate. It is convenient to introduce the distance h_j of the

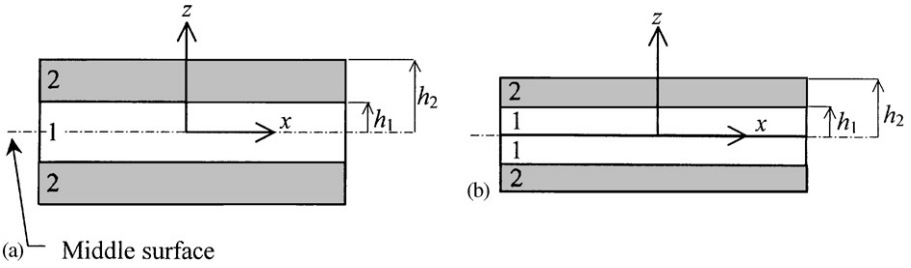

Fig. 20. Symmetric laminated composite shell showing distance h_j of the upper surface of the j lamina from the middle surface of the shell and numeration of layers of half-laminate: (a) Shell with odd number of laminae; (b) shell with even number of laminae.

upper surface of the j-lamina form the middle surface of the shell, see Fig. (20), where $j = 1, \cdots, H$ and H is the total number of layers of the half-laminate (the central half-lamina in a laminate with odd number of layers counts for one). For a laminate with an even number of laminae, the first surface of the half-laminate coincides with the middle surface of the shell and is not considered. The expression of the strain energy for this laminated composite shell is obtained as a generalization of Eq. (A.3)

$$
\begin{aligned}
U_S = & \sum_{j=1}^{H} \frac{E_{x_j}(h_j - h_{j-1})}{1 - \nu_{\theta x_j}^2 E_{x_j}/E_{\theta_j}} \int_0^{2\pi} \int_0^L \left[\varepsilon_{x,0}^2 + \frac{E_{\theta_j}}{E_{x_j}} \varepsilon_{\theta,0}^2 + 2\nu_{\theta x_j} \varepsilon_{x,0} \varepsilon_{\theta,0} + \frac{G_{x\theta_j}}{E_{x_j}} \left(1 - \nu_{\theta x_j}^2 \frac{E_{x_j}}{E_{\theta_j}} \right) \gamma_{x\theta,0} \right] \mathrm{d}x R \, \mathrm{d}\theta \\
& + \sum_{j=1}^{H} \frac{E_{x_j}(h_j^3 - h_{j-1}^3)}{3\left(1 - \nu_{\theta x_j}^2 E_{x_j}/E_{\theta_j} \right)} \int_0^{2\pi} \int_0^L \left[k_x^2 + \frac{E_{\theta_j}}{E_{x_j}} k_\theta^2 + 2\nu_{\theta x_j} k_x k_\theta + \frac{G_{x\theta_j}}{E_{x_j}} \left(1 - \nu_{\theta x_j}^2 \frac{E_{x_j}}{E_{\theta_j}} \right) k_{x\theta} \right] \mathrm{d}x R \, \mathrm{d}\theta \\
& + \sum_{j=1}^{H} \frac{2E_{x_j}(h_j^3 - h_{j-1}^3)}{3R\left(1 - \nu_{\theta x_j}^2 E_{x_j}/E_{\theta_j} \right)} \int_0^{2\pi} \int_0^L \left[\varepsilon_{x,0} k_x + \frac{E_{\theta_j}}{E_{x_j}} \varepsilon_{\theta,0} k_\theta + \nu_{\theta x_j} \varepsilon_{x,0} k_\theta + \nu_{\theta x_j} \varepsilon_{\theta,0} k_x \right. \\
& \left. + \frac{G_{x\theta_j}}{E_{x_j}} \left(1 - \nu_{\theta x_j}^2 E_{x_j}/E_{\theta_j} \right) \varepsilon_{x\theta,0} k_{x\theta} \right] \mathrm{d}x R \, \mathrm{d}\theta, \qquad \text{(A.4)}
\end{aligned}
$$

where $h_0 = 0$ and the subscript j refers to the material properties of the j-lamina. Eq. (A.4) uses Love's first approximation assumptions.

References

[1] M. Amabili, M.P. Païdoussis, Review of studies on geometrically non-linear vibrations and dynamics of circular cylindrical shells and panels, with and without fluid-structure interaction, Applied Mechanics Reviews, accepted for publication.

[2] D.A. Evensen, Non-linear flexural vibrations of thin-walled circular cylinders, NASA TN D-4090, 1967.

[3] E.H. Dowell, C.S. Ventres, Modal equations for the non-linear flexural vibrations of a cylindrical shell, International Journal of Solids and Structures 4 (1968) 975–991.

[4] J.C. Chen, C.D. Babcock, Non-linear vibration of cylindrical shells, American Institute of Aeronautics and Astronautics Journal 13 (1975) 868–876.

[5] V.D. Kubenko, P.S. Koval'chuk, T.S. Krasnopol'skaya, Effect of initial camber on natural non-linear vibrations of cylindrical shells, Soviet Applied Mechanics 18 (1982) 34–39.
[6] M. Amabili, F. Pellicano, M.P. Païdoussis, Non-linear vibrations of simply supported, circular cylindrical shells, coupled to quiescent fluid, Journal of Fluids and Structures 12 (1998) 883–918.
[7] M. Amabili, F. Pellicano, M.P. Païdoussis, Non-linear dynamics and stability of circular cylindrical shells containing flowing fluid Part I: stability, Journal of Sound and Vibration 225 (1999) 655–699.
[8] M. Amabili, F. Pellicano, M.P. Païdoussis, Non-linear dynamics and stability of circular cylindrical shells containing flowing fluid, Part II: large-amplitude vibrations without flow, Journal of Sound and Vibration 228 (1999) 1103–1124.
[9] M. Amabili, F. Pellicano, M.P. Païdoussis, Non-linear dynamics and stability of circular cylindrical shells containing flowing fluid Part. III: truncation effect without flow and experiments, Journal of Sound and Vibration 237 (2000) 617–640.
[10] M. Amabili, Theory and experiments for large-amplitude vibrations of empty and fluid-filled circular cylindrical shells with imperfections, Journal of Sound and Vibration 262 (2003) 921–975.
[11] A.A. Popov, J.M.T. Thompson, F.A. McRobie, Chaotic energy exchange through auto-parametric resonance in cylindrical shells, Journal of Sound and Vibration 248 (2001) 395–411.
[12] J. Mayers, B.G. Wrenn, On the non-linear free vibrations of thin circular cylindrical shells, Developments in Mechanics Proceedings of the th Midwestern Mechanics Conference, Johnson Publishing Co, New York; 1967, pp 819-846.
[13] H. Radwan, J. Genin, Non-linear modal equations for thin elastic shells, International Journal of Non-Linear Mechanics 10 (1975) 15–29.
[14] K.K. Raju, G.V. Rao, Large-amplitude asymmetric vibrations of some thin shells of revolution, Journal of Sound and Vibration 44 (1976) 327–333.
[15] A. Maewal, Miles' evolution equations for axisymmetric shells: simple strange attractors in structural dynamics, International Journal of Non-Linear Mechanics 21 (1986) 433–438.
[16] A. Maewal, Finite element analysis of steady non-linear harmonic oscillations of axisymmetric shells, Computer Methods in Applied Mechanics and Engineering 58 (1986) 37–50.
[17] P.B. Gonçalves, R.C. Batista, Non-linear vibration analysis of fluid-filled cylindrical shells, Journal of Sound and Vibration 127 (1988) 133–143.
[18] I.V. Andrianov, E.G. Kholod, V.I. Olevsky, Approximate non-linear boundary value problems of reinforced shell dynamics, Journal of Sound and Vibration 194 (1996) 369–387.
[19] A. Selmane, A.A. Lakis, Influence of geometric non-linearities on free vibrations of orthotropic open cylindrical shells, International Journal for Numerical Methods in Engineering 40 (1997) 1115–1137.
[20] A.A. Lakis, A. Selmane, A. Toledano, Non-linear free vibration analysis of laminated orthotropic cylindrical shells, International Journal of Mechanical Sciences 40 (1998) 27–49.
[21] J.H. Ginsberg, Large amplitude forced vibrations of simply supported thin cylindrical shells, Journal of Applied Mechanics 40 (1973) 471–477.
[22] L.J. Mente, Dynamic non-linear response of cylindrical shells to asymmetric pressure loading, American Institute of Aeronautics and Astronautics Journal 11 (1973) 793–800.
[23] C. Sansour, P. Wriggers, J. Sansour, Non-linear dynamics of shells: theory, finite element formulation, and integration schemes, Non-linear Dynamics 13 (1997) 279–305.
[24] C. Sansour, W. Wagner, P. Wriggers, J. Sansour, An energy-momentum integration scheme and enhanced strain finite elements for the non-linear dynamics of shells, International Journal of Non-Linear Mechanics 37 (2002) 951–966.
[25] J.N. Reddy, K. Chandrashekhara, Geometrically non-linear transient analysis of laminated, doubly curved shells, International Journal of Non-Linear Mechanics 20 (1985) 79–90.
[26] S.T. Dennis, AGalerkin solution to geometrically non-linear laminated shallow shell equations, Computers and Structures 63 (1997) 859–874.
[27] Y. Kobayashi, A.W. Leissa, Large-amplitude free vibration of thick shallow shells supported by shear diaphragms, International Journal of Non-Linear Mechanics 30 (1995) 57–66.
[28] N. Yamaki, Elastic Stability of Circular Cylindrical Shells, North-Holland, Amsterdam, 1984.

[29] B. Budiansky, Notes on non-linear shell theory, American Society of Mechanical Engineers Journal of Applied Mechanics 35 (1968) 393–401.
[30] V.V. Novozhilov, Foundations of the Non-linear Theory of Elasticity, Graylock Press, Rochester;, 1953.
[31] J.L. Sanders Jr.,, Non-linear theories for thin shells, Quarterly of Applied Mathematics 21 (1963) 21–36.
[32] W.T. Koiter, On the non-linear theory of thin elastic shells. I, II, III, Proceedings Koninklijke Nederlandse Akademie van Wetenschappen B69 (1966) 1–54.
[33] A.W. Leissa, Vibration of Shells, NASA SP-288, Government Printing Office, Washington, DC, Now available from The Acoustical Society of America (1993), 1973.
[34] F. Pellicano, M. Amabili, M.P. Païdoussis, Effect of the geometry on the non-linear vibration of circular cylindrical shells, International Journal of Non-Linear Mechanics 37 (2002) 1181–1198.
[35] A.A. Lakis, A. Laveau, Non-linear dynamic analysis of anisotropic cylindrical shells containing a flowing fluid, International Journal of Solids and Structures 28 (1991) 1079–1094.
[36] S. Wolfram, The Mathematica Book, 4th Edition, Cambridge University Press, Cambridge, UK, 1999.
[37] E.J. Doedel, A.R. Champneys, T.F. Fairgrieve, Y.A. Kuznetsov, B. Sandstede, X. Wang, AUTO 97 Continuation and Bifurcation Software for Ordinary Differential Equations (with HomCont), Concordia University, Montreal, Canada, 1998.
[38] T.K. Varadan, G. Prathap, H.V. Ramani, Non-linear free flexural vibration of thin circular cylindrical shells, American Institute of Aeronautics and Astronautics Journal 27 (1989) 1303–1304.
[39] M. Ganapathi, T.K. Varadan, Large-amplitude vibrations of circular cylindrical shells, Journal of Sound and Vibration 192 (1996) 1–14.
[40] I.M. Daniel, O. Ishai, Engineering Mechanics of Composite Materials, Oxford University Press, New York, USA, 1994.